VOLCANICA Article in Press

This is an uncorrected proof, meaning that this manuscript has not been copyedited or formatted according to Volcanica's styles and standards. In turn, this means that article content, including text, may still change prior to final publication. Although articles in press do not have all bibliographic details available yet, they can be cited using the year of online publication and the DOI, as follows: author(s)(year), article title, Volcanica, DOI.

Clunes, M., Lovell, H. and King, O. (2026) "Accelerated deglaciation of an ice-filled caldera promotes tensile stress conditions favourable to magma ascent", *Volcanica*, 9(2). doi: 10.30909/vol/cild9500.

Article in Press

Glacier unloading effects on stress redistribution above magma bodies in ice-filled volcanoes

Matías Clunes[*1,2], Harold Lovell[3,4], and Owen King[5]
[1]Laboratory for Deep Mining Geoscience and Engineering, Facultad de Ciencias Físicas y Matemáticas,
[2]Sociedad Chilena de Socioecología y Etnoecología (SOSOET), Chile
[3]School of the Environment and Life Sciences, University of Portsmouth, Portsmouth, United Kingdom
[4]Institute of the Earth and Environment, University of Portsmouth, Portsmouth, United Kingdom
[5]School of Geography, Politics and Sociology, Newcastle University, Newcastle, United Kingdom

[*] matias.clunes@uchile.cl [corresponding author]
ORCiD (FA): 0000-0003-4565-3235
ORCiD (SA): 0000-0002-9435-3178
ORCiD (TA): 0000-0003-1807-9821

Keywords: Accelerated glacier thinning; Glacier unloading; Tensile stress; Magma ascent; Finite Element Method; Sollipulli

Abstract

Climate warming is accelerating glacier thinning and altering the mechanics of ice-capped volcanic systems. At Sollipulli volcano (Southern Andes), digital elevation model (DEM) differencing between 1979 and 2013 reveals up to ~300 m of surface lowering and motivates a parameterized trajectory of accelerated thinning. Finite Element Method models show that cumulative ice loss reduces the minimum principal stress above a pressurized magma source and promotes upward expansion of a tensile domain. These effects are strongest for shallower sources and are amplified by magma overpressure. Within a linear elastic framework, stress changes are controlled by unloading magnitude, while different thinning trajectories produce distinct sequences of incremental stress changes, illustrated here through comparison of observed and modelled thinning histories. Thick, caldera-filling glaciers therefore enhance the mechanical sensitivity of the shallow crust to climate-driven ice loss, with implications for fracture opening, magma ascent, and volcanic hazards. Our findings suggest that currently thin glaciers may pose a disproportionately higher mechanical hazard to volcanic stability compared to their earlier, intact states.

Article in Press

Second-language abstract

El calentamiento climático está acelerando el adelgazamiento glaciar y modificando las condiciones mecánicas de sistemas volcánicos cubiertos por hielo. En el volcán Sollipulli (Andes del Sur), la diferencia entre modelos digitales de elevación de 1979 y 2013 revela hasta ~300 m de descenso superficial y motiva una trayectoria parametrizada de adelgazamiento acelerado. Modelos de Elementos Finitos muestran que la pérdida acumulada de hielo reduce el esfuerzo principal mínimo sobre una fuente magmática presurizada y favorece la expansión ascendente de un dominio tensional. Estos efectos son más intensos para fuentes más someras y se amplifican con la sobrepresión magmática. En un marco elástico lineal, los cambios de esfuerzo dependen de la magnitud del deshielo, mientras que su aceleración adelanta el momento en que se alcanzan estados mecánicamente significativos. Los resultados destacan que glaciares gruesos que rellenan calderas pueden aumentar la sensibilidad mecánica de la corteza somera frente a la pérdida de hielo, con implicancias para la apertura de fracturas, el ascenso de magma y la peligrosidad volcánica.

Introduction

In a warming climate, thinning and retreating glaciers are rapidly altering the mechanical conditions of the Earth's crust in high-latitude and high-elevation regions, including under ice sheets (Zemp et al. 2019; Hugonnet et al. 2021; The GlaMBIE Team 2025). These changes have important consequences for volcanic systems located beneath ice masses, where the removal of surface loads can modify crustal stress and potentially influence magma migration (e.g., Sigvaldason et al. 1992; Jellinek et al. 2004; Pagli et al. 2008; Sigmundsson et al. 2013). Similar associations have been observed in continental settings. For example, Glazner et al. (1999) documented an anticorrelation between glacial periods and eruptive activity in eastern California over the past 800,000 years, suggesting that surface loading from glaciers may suppress volcanism in intraplate regions, an interpretation later supported by mechanical modelling linking progressive crustal unloading to stress conditions favourable for magma ascent (Jellinek et al. 2004). This sensitivity is supported by evidence linking deglaciation and snow or ice load reduction to increased eruptive activity in regions such as Iceland (e.g., Albino et al. 2010; Sigmundsson et al. 2010), Alaska (e.g., Praetorius et al. 2016), the Garibaldi Volcanic Belt in western Canada (Wilson and Russell 2020), West Antarctica (Coonin et al. 2024), and the Andes (e.g. Rivera and Bown 2013; Van Wyk de Vries et al. 2022; Moreno-Yaeger et al. 2024, 2025). In fact, glaciers in the southern Andes (37°-46°S) are undergoing rapid and accelerating ice loss (e.g., Dussaillant et al. 2019; Hugonnet et al. 2021; Carrivick et al. 2024), with ice-capped

Article in Press

stratovolcanoes and ice-filled calderas in the region losing on average 38.8% (range: 18.6-82.7%) of their glacier area since the 1960s and 1970s (Rivera and Bown 2013; Reinthaller et al. 2019; Daros Idalino et al. 2020).

The removal of overlying ice reduces the lithostatic load, which can lead to stress changes in the crust surrounding magma bodies (e.g., Pinel et al. 2007; Tuffen 2010; Hooper et al. 2011; Sigmundsson et al. 2013; Watt et al. 2013; Mora and Tassara 2019; Singer et al. 2024; Moreno-Yaeger et al. 2025; Wanket et al. 2025). Depending on the initial stress state, such unloading may either reduce compression and promote tensile failure (as in cases of thick overburden) or decrease pre-existing tension resulting from flexural bending, particularly when the magmatic system is shallow enough for surface loads to induce bending stresses in the roof region (Pinel and Jaupart 2005). These mechanical effects can be especially pronounced in glacier-filled calderas, where thick ice masses sit directly above shallow magmatic systems and unloading is concentrated over a relatively small footprint, potentially focusing stress changes. As deglaciation continues under ongoing climate warming (Hugonnet et al. 2021; Zekollari et al. 2025), cumulative ice loss may progressively drive stress conditions toward tensile regimes, particularly above pressurized magma bodies. These mechanical effects are especially relevant in volcanic regions with persistent magmatic activity that are currently experiencing rapid ice loss, such as in the southern Andes (Rivera and Bown 2013). Prehistoric eruptive records suggest that deglaciation has previously influenced volcanic activity in the Southern Volcanic Zone (SVZ) in the Andes, with eruption frequencies during the early post-glacial period being higher than during the mid-Holocene, consistent with enhanced volcanic activity following Late Pleistocene ice retreat after the Last Glacial Maximum (Watt et al. 2013).

Beyond individual volcanic systems, the climatic relevance of these interactions has been highlighted by global-scale studies linking deglaciation to increased volcanic activity and atmospheric CO_2 release (Huybers and Langmuir 2009), suggesting that ice loss could trigger geophysical feedback with broader environmental consequences. These patterns point to a potential link between surface mass loss and enhanced volcanic response, likely mediated by changes in crustal stress. This transition has important implications for magma transport: while compressive stress can inhibit dyke propagation by promoting dyke arrest and sill formation, tensile stress conditions facilitate dyke opening and upward magma migration (Rubin 1995; Gudmundsson et al. 2002). More generally, a growing body of work has shown that magma ascent and dyke pathways are highly sensitive to externally imposed stress perturbations acting from the surface or lithosphere, highlighting a top-down mechanical control on volcanism (e.g., Maccaferri et al. 2014; Ferrante et al. 2024; Rivalta and Chamberlain 2025). Although these studies focus on crustal unloading in extensional and rift settings rather than glaciated volcanoes, they

Article in Press

illustrate a general mechanical principle directly relevant here: progressive surface unloading can reorganize the local stress field and modulate the conditions for magma ascent. In addition, changes in the stress field may be accompanied by surface deformation, including uplift or subsidence, that can be detected by geodetic techniques, such as Interferometric Synthetic Aperture Radar (InSAR) and Global Navigation Satellite System (GNSS) (e.g., Richter et al. 2016; Delgado et al. 2018; Wang et al. 2025), offering valuable insights into subsurface processes. Despite this, the mechanical implications of accelerated thinning in thick, caldera-filling glaciers remain underexplored, particularly regarding how such unloading histories influence stress evolution above shallow magmatic systems. While several studies have reviewed the diverse ways climate change may influence volcanic systems, from glacier recession to permafrost degradation and sea-level changes (e.g., Jellinek et al., 2004; Watt et al., 2013; Satow et al. 2021; Singer et al. 2024; Sottili and Palladino 2025, Moreno-Yaeger et al. 2025), the mechanical links between these processes and crustal stress evolution are only beginning to be quantified (e.g., Aubry et al. 2022). As emphasized by Tuffen (2010), understanding how deglaciation affects magma ascent and volcanic hazards is a key challenge in the context of ongoing climate change. This is particularly relevant for systems hosting thick, caldera-filling glaciers, where unusually large and spatially concentrated ice loads make unloading effects more mechanically significant.

Previous studies have demonstrated that ice unloading can promote tensile stress conditions above magmatic systems (e.g., Pinel and Jaupart 2005; Albino et al. 2010; Sigmundsson et al. 2013; Watt et al. 2013; Mora and Tassara 2019; Moreno-Yaeger et al. 2025). However, the sensitivity of shallow magmatic systems to glacier unloading likely depends strongly on the geometry of the overlying ice load, the depth of the magma body, the magnitude of magma overpressure, and the thinning trajectory of the glacier. These controls may be especially important in glacier-filled calderas, where thick and spatially concentrated ice loads are removed directly above the volcanic system. A key unresolved question is how such unloading modifies the stress field above shallow magma bodies and promotes the transition from compressive to tensile conditions. Here, we use a series of axisymmetric Finite Element Method (FEM) models to investigate the mechanical sensitivity of shallow magmatic systems to unloading from thick, caldera-filling glaciers and to evaluate how glacier geometry, source depth, magma overpressure, and thinning trajectory influence the evolution of the overlying stress field. Within this elastic framework, stress changes scale with the magnitude of ice thickness loss, whereas differences in thinning trajectories primarily control the timing at which a given stress state is reached rather than the magnitude of the stress change itself. The models represent glacier-filled calderas in which ice infill of different thicknesses imposes a near-uniform load directly above the magma body, as observed in parts of the SVZ in the Andes, including

Article in Press

Sollipulli, Michinmahuida, and Hudson (Rivera and Bown 2013). This approach isolates the roles of unloading magnitude, glacier geometry, magma overpressure, and thinning trajectory in driving the transition from compressive to tensile stress regimes, with implications for dyke propagation. The results provide first-order mechanical insights into glacier-volcano interactions, with relevance for hazard assessment in ice-capped volcanic regions, particularly in settings hosting thick, caldera-filling glaciers.

Methods

Glacier surface elevation changes and thinning rates

To estimate the magnitude of recent ice loss over the glaciated portions of the SVZ we generated digital elevation models (DEMs) of the area from declassified Hexagon KH9 images acquired on the 26th March 1979. We generated DEMs from Hexagon KH9 imagery using SpyMicMac, a set of Python-based tools that prepares historical imagery for further photogrammetric processing in MicMac (Rupnik et al. 2017). We then differenced the Hexagon KH9 DEM from the Copernicus GLO-30 DEM (hereafter COP GLO-30 DEM), which was generated from TanDEM-X acquisitions between 2011 and 2015. We adopted the central date of this acquisition window (2nd July 2013) for the purpose of estimating a rate of elevation change between the Hexagon KH9 DEMs and COP GLO-30 DEM. We followed established techniques (xDEM contributors 2023) to coregister the different DEMs and account for geolocation errors resulting from DEM misalignment. Following DEM differencing we filtered resulting elevation change data, retaining elevation change estimates where MicMac image correlation scores were greater than 60%, effectively removing portions of the Hexagon KH9 DEMs where image contrast was poor and derived elevation estimates unreliable. This filtering results in locally patchy coverage, visible as white areas in Figure 2a, corresponding mainly to steep or low-contrast regions where stereo correlation failed. To estimate the uncertainty associated with glacier surface elevation change measurements, we follow the methods developed by Hugonnet et al. (2022). These methods quantify the heteroscedasticity of elevation measurements, their variability in relation to terrain attributes such as slope and curvature, as well as the spatial autocorrelation of elevation errors, which can occur over a variety of scales. Glacier area at the time of the Hexagon acquisitions, which is a requirement for both DEM coregistration, and elevation change uncertainty calculations, was digitised manually using RGI 7.0 (RGI 7.0 Consortium 2023) as a baseline and the 1979 orthoimages as reference of glacier extent at the time.

Article in Press

Numerical modelling setup

Building upon these observation-based thinning estimates, a series of axisymmetric FEM models was developed to evaluate how glacier unloading and magma overpressure affect the stress field above a pressurized shallow magma body (Figure 1). Pressurized magma body (pressure source) depths of 2 km and 4 km were considered, representing very shallow and shallow upper-crustal conditions, respectively. The simulations were conducted in COMSOL Multiphysics 6.2 assuming a linear elastic crustal rheology, with a Young's modulus (E) of 40 GPa and a Poisson's ratio (v) of 0.25, consistent with estimates for the upper crust in volcanic arc settings (e.g., Gudmundsson 2012; Hickey and Gottsmann 2014). The model geometry consists of a cylindrical domain 20 km deep and 40 km wide, representing the upper crust, and chosen to minimize boundary effects (Hickey and Gottsmann 2014). Boundary conditions include a fixed base, roller constraints on the lateral edge (zero horizontal displacement), and a stress-free top surface where glacier loads are applied. These boundary conditions were selected to minimise artificial boundary effects and to isolate stress perturbations associated with surface loading and unloading. The fixed base represents a mechanically stiff lower boundary at depth, the lateral roller conditions approximate lateral symmetry and prevent rigid-body translation of the domain, and the stress-free top surface allows direct application of glacier loading and unloading. The domain was discretized using triangular finite elements. Mesh refinement was applied in regions of high stress gradients, including the vicinity of the pressurized magma body, along the axis of symmetry, and near the free surface where glacier loads are imposed, while a coarser mesh was used in the far field to reduce computational cost without compromising accuracy.

A spherical magma body (pressure source) was centred below the symmetry axis at depths of 2 km and 4 km (e.g., Kratzmann et al. 2009; Freundt et al. 2025) with a radius of 0.5 km (Mogi 1958; Hickey and Gottsmann 2014). In overpressurized scenarios, a constant magma overpressure (p_o) of 10 MPa was applied to the magma body boundary, with additional simulations run at 0, 5 and 20 MPa for comparison (e.g., Gudmundsson 2006; Bonaccorso et al. 2010). Glacier load was implemented as a vertical pressure applied over a circular area at the surface, representing the footprint of an ice cap centred on the volcanic edifice. Three idealized glacier footprints were modelled: one with a radius of 5 km (~80 km^2) and two with a radius of 2.5 km (~20 km^2). Initial ice thicknesses values (h_0) are set to 250 m for the 5000 m-radius case, representing broad ice-caps with low vertical accumulation (e.g., Michinmahuida), 400 m for one of the 2500 m-radius cases, representing an ice-filled caldera of moderate ice thickness (e.g., Mocho-Choshuenco), and 750 m for the other 2500 m-radius case, representing a thick ice-filled caldera (e.g., Sollipulli). These thicknesses were selected to represent a range of glacier geometries

Article in Press

and loading magnitudes informed by geophysical measurements, regional inventories, and global-scale thickness models (Rivera and Bown 2013; Farinotti et al. 2019; Edwards et al. 2020; Arndt et al. 2026).

Although the model does not incorporate glacier flow dynamics or detailed ice rheology (e.g., Bahr et al. 2014), it provides a tractable and mechanically meaningful framework for quantifying stress changes associated with progressive glacial unloading. The focus is on glacier geometries compatible with low-relief volcanic edifices, such as calderas, where ice can accumulate to considerable thickness in confined summit areas. These morphologies are simplified to the axisymmetric, flat-surface model employed in this study. By contrast, steep-sided, ice-capped stratovolcanoes tend to host thinner, more distributed ice covers because of their conical geometry and efficient outward flow, resulting in lower effective ice loads and weaker mechanical coupling with the crust (Edwards et al. 2020). Accordingly, such systems are not explicitly represented in this study, which instead focuses on configurations where glacier unloading is expected to exert a comparatively strong mechanical influence on the shallow stress field.

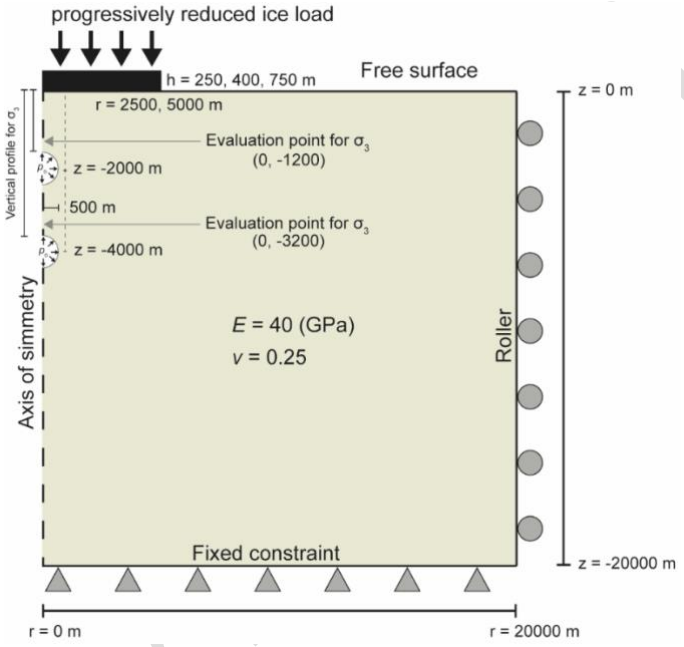

Figure 1: Axisymmetric Finite Element Method model of a pressurized shallow magma body beneath a glacier undergoing progressive unloading. The glacial load is applied as a vertical pressure over a circular area with radius r = 2500 or 5000 m, representing glaciers of different spatial extent. The unloading is implemented in incremental stages, corresponding to successive fractions of ice-thickness loss. A constant magma overpressure (p_o) of 5, 10 or 20 MPa is applied to the boundary of a spherical body of 500 m radius and centred at 2000 m and 4000 m depth, embedded in a linear elastic crust (20 km-deep and 40 km-wide) with Young's Modulus E = 40 GPa and Poisson's ratio v = 0.25. The minimum principal stress (σ_3) is evaluated above the magma body at 1200 m and 3200 m depth

and along a vertical profile from the surface to the top of the body. Boundary conditions include a fixed base, roller lateral boundary, and a free surface.

For each glacier geometry and source depth, simulations were run both without magma overpressure and with magma overpressures of 5, 10, and 20 MPa, resulting in a total of 24 model runs summarized in Table 1. The minimum principal stress (σ_3) above the pressurized magma body and the trajectories of maximum principal stress (σ_1) were extracted to assess stress changes relevant to magmatic intrusion. All results are analysed as a function of progressive ice loss during deglaciation.

Table 1: Summary of numerical model runs evaluating the crustal stress response above a pressurized shallow magma body under different glacier thinning scenarios. Each model is defined by the initial glacier thickness (h_0), glacier radius (r), with dimensions estimated from published data (Rivera and Bown 2013), magma overpressure p_o, and depth to the centre of the magma body (z).

Model run	h_0 (m)	r (m)	p_o (MPa)	z (m)	Modelled glacier geometry
A1	250	5000	0	2000	Broad ice cap (e.g., Michinmahuida)
A2	250	5000	0	4000	
B1	250	5000	5	2000	
B2	250	5000	5	4000	
C1	250	5000	10	2000	
C2	250	5000	10	4000	
D1	250	5000	20	2000	
D2	250	5000	20	4000	
E1	400	2500	0	2000	Moderate thickness ice-filled caldera (e.g., Mocho-Choshuenco)
E2	400	2500	0	4000	
F1	400	2500	5	2000	
F2	400	2500	5	4000	
G1	400	2500	10	2000	
G2	400	2500	10	4000	
H1	400	2500	20	2000	
H2	400	2500	20	4000	
I1	750	2500	0	2000	Thick caldera-filling glacier (e.g., Sollipulli)
I2	750	2500	0	4000	
J1	750	2500	5	2000	
J2	750	2500	5	4000	
K1	750	2500	10	2000	
K2	750	2500	10	4000	
L1	750	2500	20	2000	
L2	750	2500	20	4000	

Article in Press

Results

Recent glacier thinning at Sollipulli glacier-filled caldera

Progressive glacier thinning has been observed in several volcanic systems in the Southern Andes, with implications for stress redistribution in the upper crust and the mechanical stability of shallow magmatic systems. At Sollipulli, a glacier-filled ~4 km-wide caldera located in the central sector of the Andean SVZ (38.97°S, 71.52°W), elevation differences, reveal a maximum surface lowering of approximately ~320 m at the summit area between 1979 and approximately 2013 (Figure 2a). The DEM-derived elevation changes reveal a spatially heterogeneous pattern of surface change across the glacier at Sollipulli, dominated by net surface lowering. Local maximum elevation decreases exceed ~300 m near the caldera centre, whereas the mean surface lowering between 1979 and 2013 is 94±5.7 m (Figure 2a), corresponding to an average thinning rate of -2.7±0.16 m yr^{-1} over this period. A summary of the DEM-derived elevation-change and uncertainty metrics is provided in the Supplementary Material (Table S1). Ground-penetrating radar measurements from 2013 indicate a maximum remaining ice thickness of ~750 m (Arndt et al. 2026). Cumulative observations through 2024 show ~70 m of total ice loss since 2000, with acceleration from 2.05 m/yr (2000-2015) to 4.11 m/yr (2018-2024) (Arndt et al., 2026). To explore how this observed acceleration pattern influences stress redistribution, we employ a parameterized thinning trajectory (Figure 2b,c) informed by these observational constraints.

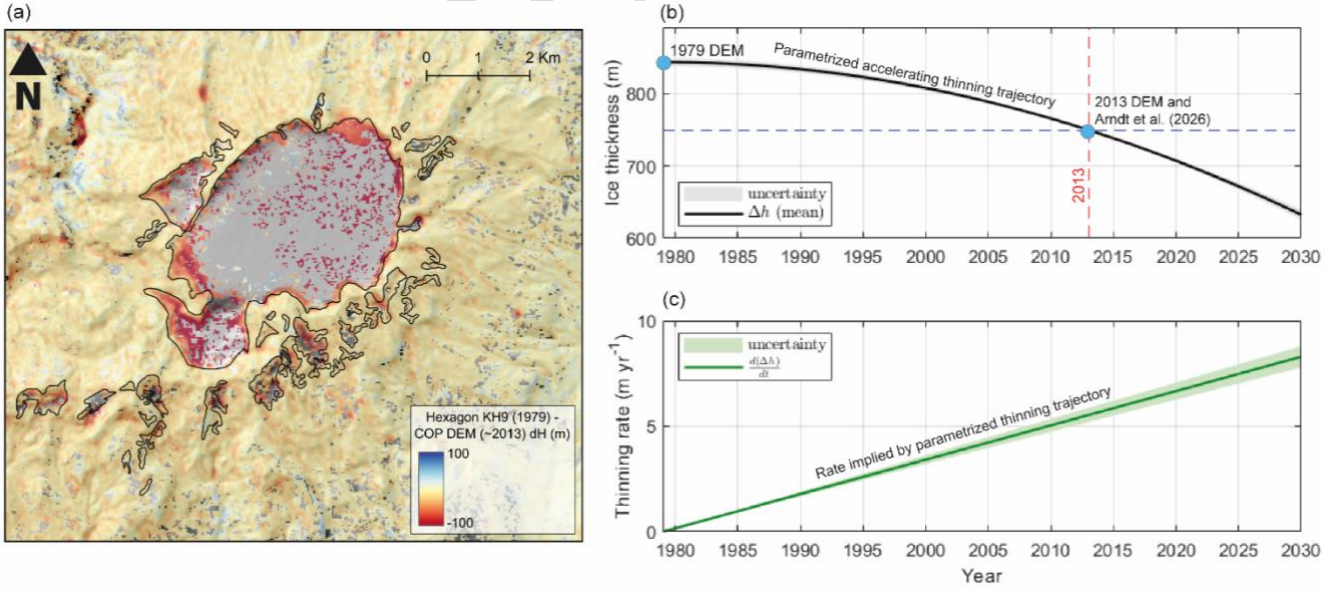

Figure 2. (a) Elevation changes in the ice-filled caldera of Sollipulli between 1979 (KH-9 DEMs) and 2013 (Copernicus DEM), overlaid on an orthoimage. Colours indicate elevation change, with negative values corresponding to surface lowering and the largest decreases concentrated near the caldera centre. (b) Parametrized thinning trajectory for Sollipulli based on observed elevation changes between 1979 and 2013. The curve represents a simple quadratic thinning trajectory used as a parameterized representation of accelerating thinning consistent with the observed magnitude of DEM-derived surface lowering. The shaded envelope indicates the mean total thickness loss (94.1 ± 5.7 m). The trajectory is anchored by the estimated maximum ice thickness in 2013 (~750 m) derived from ground-penetrating radar measurements (Arndt et al. 2026). (c) Corresponding temporal evolution of the thinning rate implied by the quadratic thinning trajectory, showing progressively increasing rates toward recent decades. Uncertainty bounds reflect the standard deviation of the total thickness loss. Data gaps, where the underlying DEM hillshade is visible, correspond to areas where stereo matching failed, or image contrast was insufficient to derive reliable elevation differences, and were excluded from the reported mean and uncertainty calculations.

Based on these observations, the magnitude of the applied pressure can be modelled as a nonlinear function that reflects the progressive loss of ice thickness (Eq. 1):

$$p(t) = \rho_{ice} \cdot g \cdot h_0(1 - f^2) \quad (1)$$

where $\rho_{ice} = 917 \frac{kg}{m^3}$, $g = 9.81 \frac{m}{s^2}$, and h_0 is the initial ice thickness defined above. The dimensionless thinning factor $f \in [0,1]$, represents the progression of ice loss, where $f = 0$ corresponds to the full initial glacier load and $f = 1$ to complete ice removal. For instance, assuming h_0 = 750 m, the glacier loses only 66 m by f = 0.3, but 367 m by f = 0.7, and 750 m by f = 1. Similar non-linear thinning patterns have been observed in temperate glaciers (Pelto et al. 2010) and across glacierized regions globally (Hugonnet et al. 2021). By varying f, we can evaluate the evolution of the stress field surrounding a shallow magma body as glacier loads progressively decrease.

Stress fields across different unloading and overpressure conditions

The Sollipulli volcanic complex hosts a ~4 km wide, ice-filled summit caldera whose formation has been interpreted as non-explosive and largely constructional, associated with prolonged glaciovolcanic activity and subsidence (Gilbert et al. 1996; Lachowycz et al. 2015). Holocene activity at Sollipulli has been dominated by

Article in Press

effusive eruptions and lava emplacement along the caldera margins and flanks, consistent with shallow to mid-crustal magma storage inferred from petrological and geochemical studies (Gilbert et al. 1996). Subsequent activity involved lava dome emplacement and effusive eruptions on the northern and southwestern flanks, suggesting the presence of a shallow and potentially reactivable magmatic system (Naranjo et al. 1993). Petrological and geochemical studies (Gilbert et al. 1996) indicate that the magmas erupted during the Holocene are predominantly dacitic and derived from mid- to upper-crustal storage zones. Recent petrological constraints from the Alpehué Plinian eruption (~3 ka), which occurred from a vent located southwest of the caldera rim, indicate magma storage at depths of ~4 km within the broader Sollipulli magmatic system (Freundt et al. 2025).

Figure 3 shows the spatial distribution of minimum principal stress (σ_3) and the orientation of the maximum principal stress (σ_1) for model scenarios with an initial ice thickness h_0 = 750 m and radius r = 2500 m (e.g., Sollipulli). The upper row panels (Figure 3a to 3f) correspond to a magma body centred at 2 km depth, while the lower row (Figure 3g to 3l) shows equivalent results for a deeper magma body centred at 4 km depth. In all panels, compressive minimum principal stresses ($\sigma_3 > 0$) are shown in red and tensile stresses ($\sigma_3 < 0$) in blue. Black lines indicate the orientation of σ_1. The panels correspond to different values of the ice volume loss fraction (f) with constant magma overpressure p_o = 10 MPa. The remaining ice thickness at each stage is shown as a light blue rectangle at the top of each panel, drawn to scale relative to the initial glacier height.

For the shallow case (2 km depth, Figure 3a to 3f), the minimum principal stress field (σ_3) is vertically oriented near the surface and becomes increasingly influenced by the presence of the magma body with depth. In the case with no unloading (f = 0, Figure 3a), a broad region of positive σ_3 (compressive regime) is located above the body, with weak stress perturbations surrounding it. Increasing the unloading to f = 0.3 and f = 0.5 (Figure 3b and 3c) results in small changes of the zone with lower σ_3 values around the body and progressive reorientation of σ_1 trajectories in the surrounding crust, from subvertical to subhorizontal and radial. When f = 0.75 (Figure 3d), the tensile stress concentration around the magma body becomes significantly more pronounced, and the orientation of σ_1 displays a more radial pattern around the magma body margins. Figure 3e (f = 0.85), highlights how non-linear glacier thinning scenarios concentrate stress changes during advanced stages of ice loss, leading to more pronounced modifications of the stress field around the pressurized shallow magma body. Figure 3f, when the ice load is fully removed (f = 1), compressive stresses associated with glacier loading vanish entirely, and σ_1 trajectories become radial throughout the crustal domain.

Article in Press

For the deeper magma body case (4 km depth; Figure 3g to 3l), the stress field exhibits a different initial configuration. At f = 0 (Figure 3g), σ_3 values above the body are already negative, indicating tensile conditions extending through a substantial portion of the upper crust. Progressive unloading to f = 0.3 and f = 0.5 (Figure 3h and 3i) primarily modifies the magnitude and spatial extent of the tensile stresses rather than inducing a transition from compression to tension. As unloading increases further (f = 0.75 and f = 0.85; Figures 3j and 3k), tensile stresses around the body intensify and extend upward, while σ_1 trajectories become increasingly radial near the body margins. In the fully unloaded case (f = 1; Figure 3l), tensile stresses dominate the region above the magma body, and σ_1 orientations are radially distributed over most of the model domain.

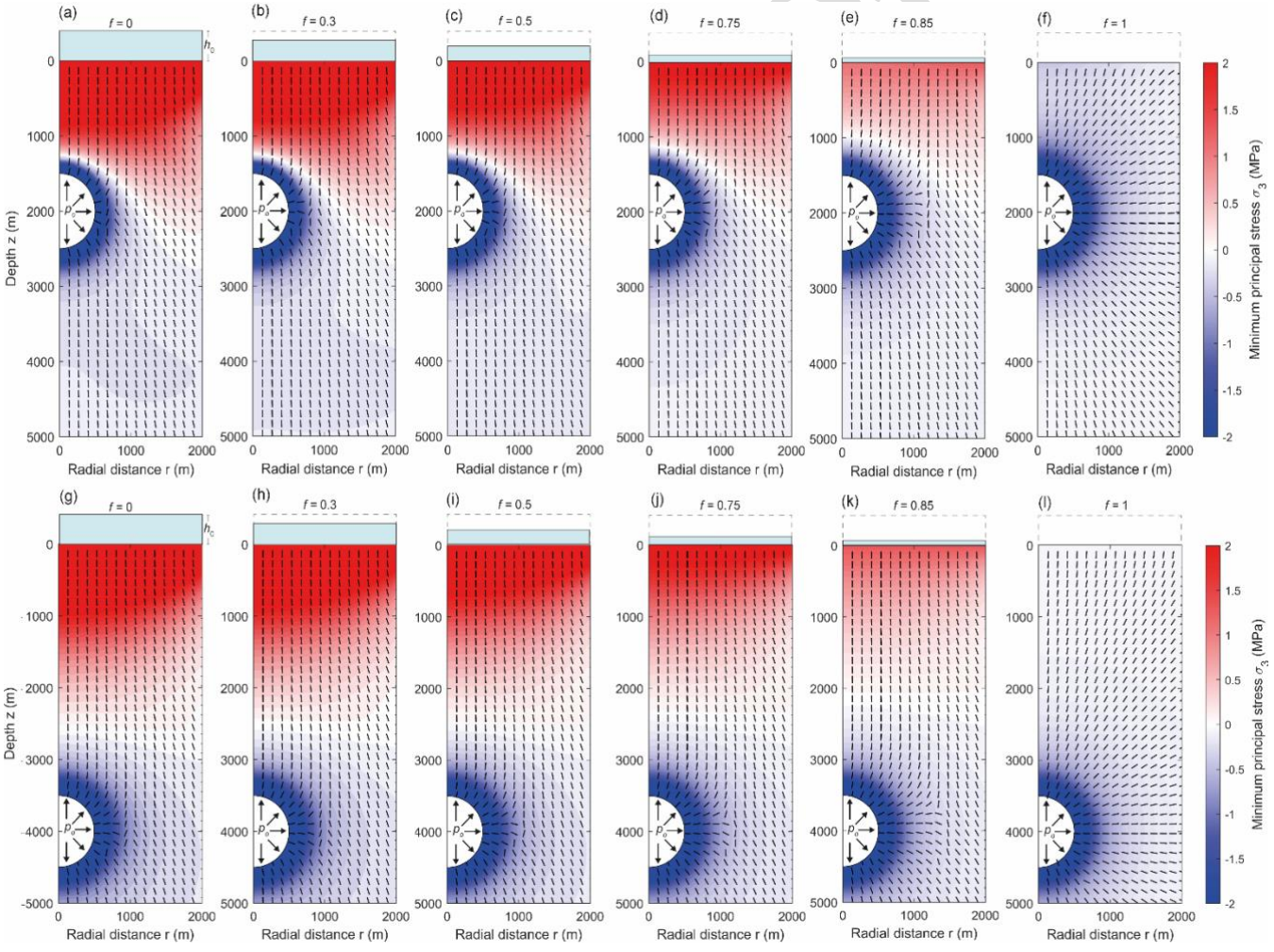

Figure 3: Minimum principal stress field (σ_3, colour scale) and orientation of the maximum principal stress (σ_1, black lines) for three scenarios with identical initial glacier geometry (h_0 = 750 m, r = 2500 m) and magma overpressure

p_o= 10 MPa from a magma body centred at 2 km (a-f) and 4 km depth (g-l). The parameter f denotes the fraction of ice volume removed due to glacier unloading. (a) f = 0, (b) f = 0.3, (c) f = 0.5, (d) f = 0.75, (e) f = 0.85, and (f) f = 1. The initial ice thickness h_0 is indicated as a dashed line, and the remaining ice is shaded in light blue. The magma body is shown as a white circle.

Stress evolution above the magma chamber

Figure 4 shows the evolution of the minimum principal stress (σ_3), evaluated at 300 m above the upper boundary of the pressurized magma body, as a function of ice thickness lost (f), for different glacier geometries and magma overpressure (p_o) scenarios, and for two depths (2 km and 4 km). Figures 4a and 4b present results for a shallow magma body centred at 2 km depth. Figure 4a illustrates the combined effects of glacier unloading and magma overpressure on σ_3 for various ice thicknesses (h_0) and glacier radii (r). In all cases, σ_3 decreases progressively with increasing f, reflecting the mechanical effect of glacier unloading. However, the magnitude of this decrease and the resulting stress regime depend critically on both the initial ice geometry (thickness and area extent) and magma overpressure.

For the 2 km depth scenario, only the thickest glacier (h_0 = 750 m) combined with magma overpressure (solid lines) begins under compressive conditions ($\sigma_3 > 0$). Continued ice thinning in these cases leads to a transition into tensile stress ($\sigma_3 < 0$), occurring earlier (at lower f) for more spatially localized glacier geometries (i.e., smaller radius). This behaviour reflects the more concentrated unloading associated with narrow, thick ice covers. In contrast, glacier-only scenarios (dashed lines) exhibit a systematic reduction in compressive stress with unloading, but do not reach tensile regime, even for thick glaciers. The role of glacier extent is also evident, as the broad but thinner glacier (h_0 = 250 m, r = 5000 m) produces a stronger initial compressive load than the thicker but more geographically-concentrated glacier with h_0 = 400 m and r = 2500 m.

Figure 4b shows the evolution of σ_3 for a fixed glacier geometry (h_0 = 750 m, r = 2500 m) under increasing magma overpressure. Increasing p_o shifts σ_3 toward lower values over the entire range of f. For $p_o \geq 10$ MPa, σ_3 becomes negative at intermediate to high values of f, whereas for p_o = 0 MPa, σ_3 remains positive for all ice thickness considered. Figures 4c and 4d present the corresponding results for a deeper pressurized magma body located at 4 km depth. In contrast to the shallower case, σ_3 values at f = 0 are negative for most glacier geometries and overpressure scenarios. In Figure 4c, variations in glacier thickness and radius produce relatively small changes in

Article in Press

σ_3 compared to the 2 km case, and σ_3 remains negative throughout the full range of f for all geometries. Differences between glacier configurations are most evident at low f and diminish as f approach 1. Figure 4d shows that increasing magma overpressure shifts σ_3 to progressively lower values, but the relative variation of σ_3 with ice thinning is limited compared to the shallower case. A notable difference between the shallower (Figure 4a) and deeper (Figure 4c) pressure source configurations is the relative ordering of glacier geometries in terms of the magnitude of σ_3 variations. While at 2 km depth the largest changes in σ_3 are associated with thicker and more localized glaciers, at 4 km depth the glacier with the largest lateral extent (h_0 = 250 m, r = 5000 m) exhibits σ_3 variations comparable to or exceeding those of thicker but narrower glaciers.

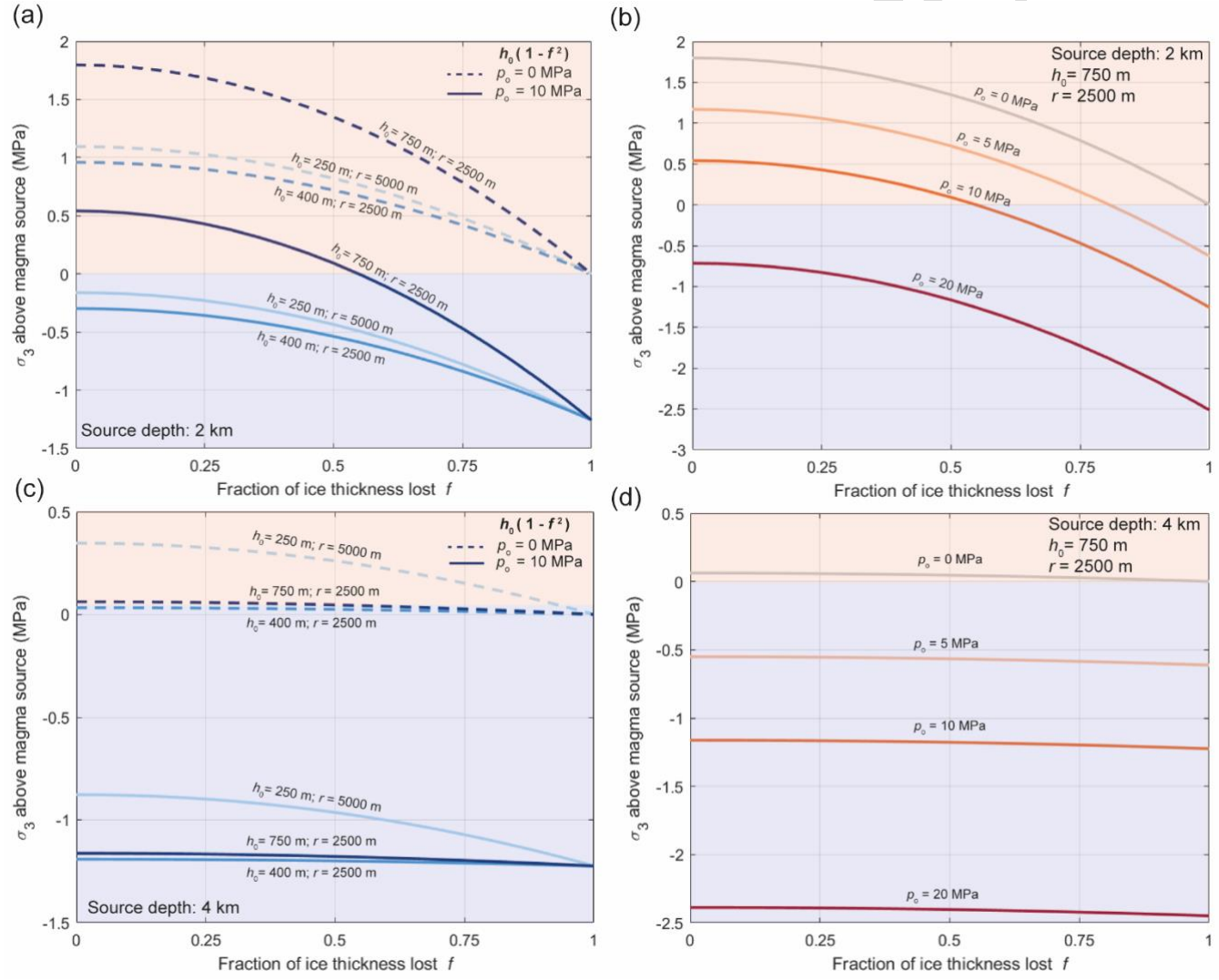

Figure 4: Evolution of the minimum principal stress (σ_3) 300 m above a pressurized magma body as a function of the fraction of ice thickness lost f, under varying glacier geometries and magma overpressure (p_o) scenarios. Background shading indicates compressive (σ_3 > 0, red) and tensile (σ_3 < 0, blue) stress regimes. (a) Results for three initial ice thicknesses (h_0 = 250, 400, 750 m), paired with glacier radii of 5000, 2500, and 2500, respectively, with magma overpressure p_o = 0 MPa (dashed lines) and p_o = 10 MPa (solid lines). Blue tones darken with increasing ice thickness. All curves correspond to a quadratic thinning history, proportional to $1 - f^2$. (b) Results for a fixed glacier geometry (h_0 = 750 m, r = 2500 m) under varying levels of magma overpressure (p_o = 0, 5, 10, 20 MPa), highlighting the increasingly tensile stress conditions promoted by higher internal pressurization during glacier thinning. (c-d) Same as (a-b), but for a deeper pressure source centred at 4 km.

Figure 5 illustrates the vertical evolution of the minimum principal stress (σ_3), incremental changes, and the development of tensile volumes above the pressure source for the case with initial ice thickness h_0 = 750 m, glacier radius r = 2500 m, and constant magma overpressure p_o = 10 MPa. Figure 5a shows vertical profiles of σ_3 above the pressure source for the 2 km depth case. For f = 0 (no unloading), σ_3 is positive above ~1275 m depth, reaching 0.67 MPa at 300 m from the source upper boundary. Progressive glacier thinning leads to a systematic decrease of σ_3 throughout the profile. The first occurrence of tensile conditions (σ_3 < 0) at 300 m above the upper boundary is at f = 0.3. By f = 0.75, σ₃ at this depth reaches –2.18 MPa, and by complete unloading (f = 1) it reaches –3.16 MPa. The vertical extent of the tensile domain increases with f. At f = 0.75, the upper limit is located at ~1260 m depth, and by f = 1 it migrates upward to ~1230 m depth. Immediately above the pressure source (1400–1500 m), σ₃ becomes slightly less negative at higher f values, producing a local inversion in the vertical stress gradient. The minimum tensile magnitude at the upper boundary of the source is –5 MPa at f = 0.75, increasing to –5.51 MPa at f = 1.0.

Figure 5d presents the equivalent σ_3 profiles for the 4 km depth case. In this configuration, σ_3 is already negative throughout the evaluated interval at f = 0, and progressive unloading results in comparatively smaller changes in σ_3 near the upper boundary of the pressurized magma body. The separation between curves corresponding to different f values is reduced relative to the 2 km case within the first 300 m above the pressure source, indicating a weaker sensitivity of near-source stresses to glacier thinning at greater source depth. Nevertheless, σ_3 continues to decrease monotonically with increasing f over the full depth range shown.

Article in Press

Figure 5b shows the incremental stress change ($\Delta\sigma_3$) between successive unloading intervals for the 2 km depth case, comparing quadratic and linear thinning histories. For the quadratic thinning scenario, the late-stage interval ($f = 0.75 \rightarrow 1$) produces the largest stress change, reaching a maximum $\Delta\sigma_3$ of -2.56 MPa at ~1306 m depth. This value is approximately 1.4 times larger than the mid-stage interval ($f = 0.5 \rightarrow 0.75$), which reaches -1.83 MPa. For the linear thinning case, $\Delta\sigma_3$ magnitudes are more evenly distributed across intervals, with the late-stage maximum (-2.17 MPa at ~1258 m) being only marginally larger than the the mid-stage value (-2.02 MPa at ~1161 m).

Figure 5e shows the corresponding incremental stress changes for the 4 km depth case. While the overall pattern of larger $\Delta\sigma_3$ values during later unloading stages is preserved, peak $\Delta\sigma_3$ magnitudes occur at greater distances above the magma body compared to the 2 km case. Within the first 300 m above the pressure source, differences between unloading intervals are comparatively small, and the strongest stress changes are shifted upward in the crust.

Article in Press

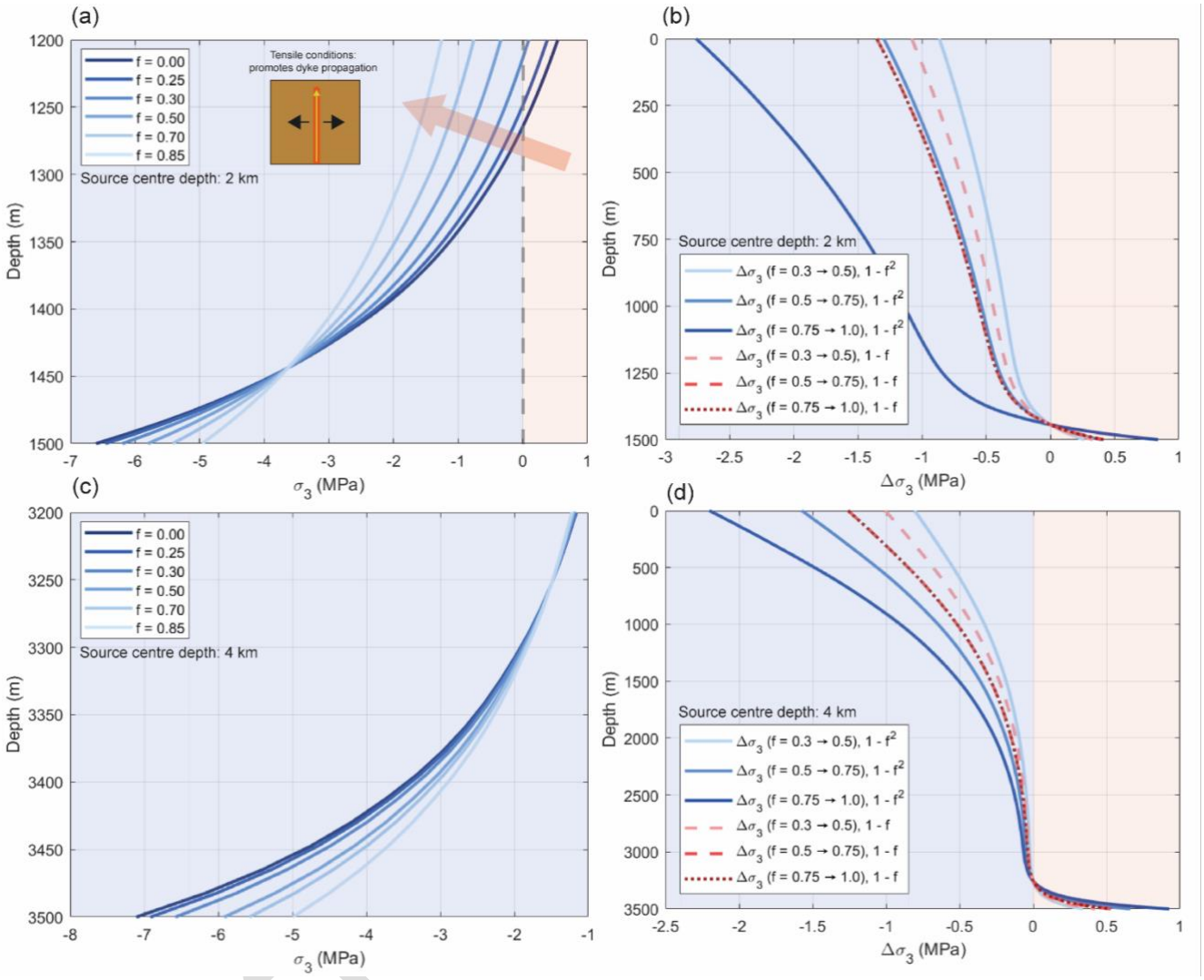

Figure 5: (a, c) Vertical profiles of the minimum principal stress (σ_3) evaluated 300 m above a pressurized magma body for progressive glacial unloading (f = 0 -1), assuming an elastic crust and a constant magma overpressure of 10 MPa. Panels (a) and (c) correspond to pressure source centre depths of 2 km and 4 km, respectively. Background shading indicates compressive (σ_3 > 0, red) and tensile (σ_3 < 0, blue) stress regimes. The red arrow schematically indicates the direction of stress evolution associated with progressive glacier unloading, highlighting the transition from compressive to tensile conditions. Inset illustrate conceptual dyke trajectories under tensile stress regime. (b, d) Depth profiles of the incremental change in minimum principal stress ($\Delta\sigma_3$) between successive stages of glacier thinning for the same configuration shown in (a) and (c). Solid lines correspond to a quadratic thinning history

(proportional to $1 - f^2$), while dashed lines represent a linear thinning scenario ($1 - f$). Three unloading intervals are shown for each case: f = 0.3-0.5, f = 0.5-0.75, and f = 0.75-1.

Discussion

Implications for magma propagation

Our results show that progressive glacier unloading can substantially modify the stress field in the upper crust above a pressurized magma body, driving an overall reduction in the minimum principal stress (σ_3) and, in some configurations, a transition from dominantly compressive ($\sigma_3 > 0$) to tensile ($\sigma_3 < 0$) conditions. Such stress regime changes define domains where mode I fracturing is mechanically favoured, creating conditions conducive to vertical dyke propagation towards the surface. Conversely, when σ_3 remains positive, tensile fracturing is suppressed and magma is more likely to propagate laterally into sills along mechanically weak horizons (Gudmundsson 2002; Galland et al. 2014). Within the linear elastic framework adopted here, the resulting stress state is controlled by the magnitude of ice unloading, whereas the rate of glacier thinning directly dictates the timing at which a given stress condition is reached.

Across the range of geometries explored, the magnitude and spatial distribution of unloading-induced stress changes depend strongly on both the depth of the magma body and the geometry of the overlying glacier. For shallower bodies, unloading produces larger stress gradients and more pronounced stress regime transitions within a few hundred metres above the source upper boundary. In contrast, for deeper pressure sources (4 km), σ_3 at the evaluation point above the source is already negative at f = 0, and progressive unloading primarily modulates the magnitude and vertical distribution of tensile stress rather than inducing a clear sign change. This indicates that glacier unloading remains mechanically relevant at greater depths, but its effects become increasingly distributed over a thicker crustal column, reducing the sharpness of near-source stress perturbations. The geometry of the ice load further modulates this response. The relative influence of ice thickness and lateral extent varies with depth: for shallower pressure sources, thick glaciers tend to produce stronger near-source stress gradients and earlier reductions in σ_3 for a given fraction of ice loss, whereas for deeper pressure sources, laterally extensive loads can exert a comparatively larger influence on σ_3 evaluated near the source.

Article in Press

A notable feature of the stress profiles in Figure 5a is the localized inversion in σ_3 immediately above the source upper boundary (1400-1500 m), where increasing unloading leads to slightly less tensile conditions. This inversion is much less pronounced for the deeper pressure source case (Figure 5c), where unloading primarily modulates the magnitude of tensile stress over a broader vertical interval rather than producing a localized stress reversal near the pressure source roof. This behaviour reflects stress relaxation associated with the combined effects of source pressurization and evolving surface loads, and highlights that the region most favourable for tensile failure is not necessariliy located directly at the source margin, but rather within an overlying volume where stress gradients are maximized. This is consistent with observations and models indicating that dykes nucleation commonly occurs above, rather than exactly at, the top of magma storage regions (e.g., Roman and Cashman 2018). Incremental stress profiles in Figures 5b and 5d further emphasize the importance of the cumulative unloading path. For non-linear (quadratic) thinning, the late stage unloading interval produces noticeably steeper stress changes than earlier stages, whereas linear thinning yields a more uniform pattern. This late-stage concentration follows directly from the increasing slope of the prescribed quadratic loading function as f approaches 1, and is therefore an expected consequence of the chosen parametrization rather than an emergent nonlinear feedback of the mechanical system. Its relevance lies in showing how a physically motivated thinning trajectory translates into a specific sequence of stress increments, rather than in the magnitude of the late-stage change per se. Such dynamics may enhance the probability of brittle failure or seismic activation once the crust approaches critical stress conditions. These findings are consistent with earlier modelling efforts by Sigmundsson et al. (2013), who showed that ice mass loss can induce stress changes sufficient to alter failure conditions and rupture potential, particularly above shallow magma bodies.

The peak stress changes modelled here range from <0.1 MPa in the deeper (4 km) pressure source scenario to a few MPa for shallower sources beneath thick, caldera-filling glaciers. Although such stress perturbations may appear modest, they fall within the range commonly considered sufficient to influence tensile fracture opening, dyke propagation, and fault reactivation in volcanic and crustal rocks (Hill et al. 2002; Toda et al. 2005; Gudmundsson 2011; Heap and Violay 2021). Moreover, static stress changes as small as ~0.01 MPa have been shown to influence seismic activity in critically stressed crustal systems (King et al. 1994; Ziv and Rubin 2000; Brown and Ge 2018). In this sense, the mechanical relevance of glacier retreat in the systems considered here lies in the unusually large and spatially concentrated ice loads involved, which allow glacier unloading to generate stress perturbations of mechanically significant magnitude in the shallow crust. Under ongoing climate warming and accelerated glacier thinning, such stress states may be reached over progressively shorter timescales, increasing

Article in Press

the potential for unloading to influence magma ascent, fracture propagation, or structural reactivation. The magnitude of unloading-induced stress changes is comparable to previous local-scale models of deglaciation-driven stress perturbations (e.g., Rawson et al. 2016; Wilson and Russell 2020; Moreno-Yaeger et al. 2025), but is up to two orders of magnitude smaller than the decompression values reported by Mora and Tassara (2019). This difference primarily reflects the contrasting physical frameworks: while Mora and Tassara (2019) model regional lithospheric flexural unbending of an elastic plate of finite thickness, leading to large-scale decompression of the upper crust, our approach focuses on local stress perturbations around a pressurized magma body in an elastic medium. As such, the stress changes reported here should be interpreted as conservative, first-order estimates of local unloading effects, rather than as full lithospheric-scale decompression. Results from Figure 4b further show that increasing magma overpressure systematically shifts σ_3 toward more tensile values, amplifying unloading-induced stress perturbations and expanding the volume affected by tensile conditions. While overpressure alone does not control the onset of tensile regimes, particularly for deeper pressure sources (Figure 4d), it enhances the magnitude of tensile stresses reached for a given amount of glacier unloading.

The present models are motivated by conditions at the glacier-filled caldera of Sollipulli, where recent constraints suggest magma storage at ~4 km depth (Freundt et al. 2025), but the results are also generally applicable to systems hosting shallower or transient magma bodies. Geophysical and petrological studies increasingly indicate that eruptible magma may reside temporarily at shallow levels prior to ascent, forming vertically extensive and mechanically unstable storage regions rather than long-lived, static chambers (Cashman et al. 2017). In such settings, surface unloading processes may exert a stronger mechanical influence on magma propagation than would be inferred from long-term average storage depths alone.

These results provide a first-order mechanical framework to interpret eruptive trends in glacierized volcanic regions in the past. In particular, Watt et al. (2013) proposed that magma stored beneath ice can be mobilized during deglaciation due to increased magmatic overpressure and upper-crustal stress conditions more favourable to dyke propagation. They argue that such responses do not require enhanced melt generation, but can be explained by changes in the mechanical stress regime. This effect is expected to become more pronounced in the later stages of glacier retreat, as cumulative ice loss brings the system closer to critical stress conditions. Pelto et al. (2010) emphasize that once the accumulation zone is affected, glaciers often transition into irreversible mass loss, a condition that may exert an increasingly dominant influence on crustal stress evolution in glaciated volcanic settings. In this sense, our models provide a first-order physical basis for this scenario, demonstrating how crustal

Article in Press

stresses evolve during thinning and identifying a key region above shallow magma bodies where brittle failure is most likely to occur.

Implications for volcanic edifice stability

Glacier unloading may also influence the long-term structural stability of volcanic edifices. Large-scale mass removal during Late Pleistocene and Holocene deglaciation has been linked to changes in eruptive behaviour and edifice stress conditions in strongly glaciated volcanic regions, particularly in Patagonia (e.g., Rawson et al. 2015, 2016; Moreno-Yaeger et al. 2024, 2025). This may also be relevant in the Southern Andes, where volcanoes such as Antuco exhibit evidence of sector collapse and were likely substantially glacierized in the past (Singer et al. 2000; Romero et al. 2023), although Antuco is located further north than the Patagonian volcanic systems mentioned above and likely experienced lower ice volumes overall. Notably, the major flank collapse at Antuco occurred 6,200 years ago, approximately 12,000 years after the end of the Last Glacial Maximum (LGM) (Martínez et al. 2018). While this temporal gap might seem large, geological evidence suggests that glaciers persisted for several millennia after the LGM in a retreating state (e.g., Mendelova et al. 2017). If glacier retreat persisted over an extended interval, progressive unloading may have contributed to gradual changes in stress conditions within the edifice, especially along pre-existing structural weaknesses or altered zones. Our models do not explore this scenario explicitly, but the stress perturbations associated with glacier thinning could have acted as a long-term contributing factor to mechanical failure. Future work integrating paleoglacial reconstructions, mechanical heterogeneities, and slope stability modelling may help quantify this potential link and assess how deglaciation influences flank collapse timing and likelihood. Moreover, given the observed acceleration of glacier retreat in many regions of the world (Hugonnet et al. 2021), including the Southern Andes, such structural destabilization processes may not be confined to the geological past, but could become increasingly relevant over the coming decades.

Regional and global perspectives

The accelerated thinning trend observed at Sollipulli is consistent with regional acceleration trends documented in the Andes of central Chile (Jo et al. 2023) and globally (Hugonnet et al. 2021). This thinning trend could also be representative of other glacier-filled summit craters such as Puyehue, in the Puyehue-Cordón Caulle volcanic complex, which thinned by nearly 300 m from 1979 to ~2013 (Figure S1). In this system, magma storage was initially interpreted to be very shallow, at depths of ~2.5-3 km, based on petrological constraints (Castro et al. 2013;

Article in Press

Seropian et al. 2021). Subsequent studies incorporating additional petrological evidence have revised the dominant storage depth to ~5-7 km (Winslow et al. 2022). Importantly, this re-estimation does not preclude the development of transient, mechanically significant intrusions at much shallower levels (e.g., Cashman et al. 2017). Indeed, geodetic and geophysical observations document the emplacement of a shallow laccolith at depths of a few hundred meters beneath the surface during the 2011-2012 eruptive cycle (Castro et al. 2016; Delgado et al. 2016, 2018). Such observations demonstrate that even in systems with deeper long-term magma storage, the stress state of the uppermost crust can be strongly influenced by short-lived, very shallow magma bodies.

In this context, the magnitude of ice loss documented at Puyehue over the observational period remains modest relative to the total ice thickness, but its temporal trajectory closely aligns with the early portion of the quadratic thinning curve similar to that explored in our models. Moreover, the timescale required to approach complete unloading is consistent with long-term loss trajectories observed in temperate and tropical regions, including cases where more than 40% of glacier volume has been lost within ~15 years (Masiokas et al. 2020). In extreme cases, some regions have effectively lost all their glaciers within decades, such as in Venezuela (Rabatel et al. 2013; Swain et al. 2024). Under such conditions, cumulative ice loss may already be sufficient to drive the crust toward tensile stress regimes in some volcanic settings, even before complete deglaciation is achieved.

The magnitude and acceleration of ice loss observed at Sollipulli (Figure 2) are consistent with the more intense unloading scenarios explored in our models. As thinning progresses and cumulative ice loss increases, our results predict the upward expansion of the tensile stress domain above pressurized magma bodies, increasing the likelihood of brittle failure in the overlying crust. It is important to note that many ice-filled calderas are infilled with thick sequences of pyroclastic deposits, which typically have lower Young's modulus and tensile strength than the surrounding edifice. Such mechanical contrasts may modify the redistribution of stresses during unloading by altering both stress magnitudes and failure thresholds, potentially changing the depth, extent, or timing of tensile failure relative to predictions from homogeneous elastic models.

Although the modeled glacier geometries used here were based on estimations of known volcanic systems, the framework that has been developed can be extended to larger ice-covered regions. This includes scenarios where active volcanic edifices are almost entirely covered by thick glacier ice, such as Lautaro beneath the Southern Patagonian Icefield (e.g., Mouginot and Rignot 2015). Similar considerations apply to remote subglacial volcanic systems, such as those identified in West Antarctica (Van Wyk de Vries et al. 2018; Coonin et al. 2024; Wanket et

Article in Press

al. 2025). In such settings, rapid glacier mass loss could drive crustal stress changes that remain undetected due to sparse monitoring networks or the subtle nature of early mechanical responses, yet still influence magma ascent or edifice stability.

These stress transitions could also influence the mechanical response of crustal structures associated with caldera systems. In particular, magma overpressure and external loading variations may perturb pre-existing faults surrounding calderas, potentially facilitating their reactivation. Recent evidence from the Southern Patagonian Icefield has shown that rapid ice-mass removal can induce measurable crustal deformation and trigger fault reactivation (Ammirati et al. 2024), underscoring the sensitivity of the brittle upper crust to surface unloading at glaciated volcanic arcs . Even moderate ice-thickness reductions were sufficient to promote slip along pre-existing discontinuities, suggesting that mechanical thresholds for reactivation can be reached under present-day deglaciation rates. Villarroel et al. (2024) similarly demonstrated that inherited structural anisotropies can localize rupture in caldera systems, with stress field configurations playing a key role in controlling the onset of ring faulting. Incorporating glacier unloading into such frameworks could help assess the mechanical conditions favoring caldera fault slip, especially under accelerating ice loss.

Our models show that vertical stress gradients induced by glacier unloading strongly control fracture localization. However, in more complex crusts, this response may interact with host-rock anisotropies, layering, or mechanical discontinuities. Previous work has demonstrated that such heterogeneities can significantly modify the trajectory of magma-driven fractures (Clunes et al. 2021; 2024) and even amplify or suppress surface displacements depending on the dip and stiffness contrast of the layers (Clunes et al. 2023). These effects suggest that crustal structure may modulate not only dyke propagation paths but also the geodetic signals associated with glacial unloading and magma ascent. Incorporating these complexities into future models could help bridge the gap between idealized mechanical predictions and the asymmetric, stratigraphy-influenced behavior observed in real volcanic systems.

Model considerations and uncertainties

The conceptual framework presented here remains a first-order mechanical approximation of the response of glacier-filled volcanic systems to accelerated surface unloading. The model neglects horizontal glacier recession and ice mass thickness variations, temperature-dependent viscoelastic relaxation of the crust surrounding magma

Article in Press

chambers, topographic complexity, and crustal heterogeneities (e.g., faults and mechanical layering), time-dependent variations in magma overpressure, comparisons between magma body geometries and magma rheology, and the presence of a regional tectonic stress field. These simplifications allow isolation of the mechanical effects of accelerated glacier thinning and enable controlled comparisons across geometries and loading scenarios. In particular, the mechanical behaviour of the host crust is simplified as that of a homogeneous, isotropic elastic medium (e.g., Mogi 1958). While this assumption facilitates comparison across scenarios, volcanic systems often exhibit significant heterogeneity in lithology, porosity, and structural fabric (e.g., Trasatti et al. 2003; Gudmundsson and Brenner 2004; Long and Grosfils 2009; Ruz et al. 2020; Heap and Violay 2021; Clunes et al. 2021). Such heterogeneities can strongly influence stress distributions, leading to localised stress amplification and preferential failure zones (e.g., Gudmundsson 2006; Clunes et al. 2024). By isolating key mechanical thresholds in a simplified medium, the present model provides a controlled reference framework against which more complex configurations can be evaluated.

A further geometric simplification of the model concerns the assumption of a flat caldera-floor topography beneath the glacier load. In natural systems, post-caldera volcanism can significantly modify caldera morphology through the emplacement of lava flows, domes, and shallow intrusions, as documented in non-glacier-filled calderas such as Crater Lake (Gardner et al. 2001), as well as in glacier-filled systems like Sollipulli (Lachowycz et al. 2015) and Mocho-Choshuenco (Moreno-Yaeger et al. 2024). Such post-caldera features may locally alter glacier thickness, surface loading distribution, and stress transfer to the underlying crust. While these complexities are not explicitly represented in the present axisymmetric models, they may influence local stress heterogeneity and fracture localization during glacier unloading and therefore represent an important aspect to be addressed in future studies.

An additional limitation of the model is the omission of a pre-existing regional tectonic stress field, which is particularly relevant for Andean volcanic systems developed within long-lived compressive to transpressive (oblique) regimes associated with Nazca-South America plate convergence (e.g., Cembrano and Lara 2009). In such settings, the regional stress field includes both compressive and shear components, leading to spatially variable stress states in the upper crust. Under the assumption of linear elasticity, superposition of glacier unloading-induced stress onto a non-zero background stress would not alter the first-order spatial pattern of stress perturbations generated by ice mass loss. However, it would modify the absolute magnitudes of the principal stresses and, consequently, the conditions under which the minimum principal stress (σ_3) may locally approach or reach tensile values. Recent studies have shown that the addition of far-field compression can locally enhance tensile stresses in

Article in Press

favourably oriented regions of the crust, while simultaneously restricting the range of principal stress orientations and dyke trajectories (e.g., Ruz et al. 2020; Drymoni et al. 2023, 2024). In transpressive tectonic regimes, regional compression does not preclude the development of local extensional conditions. Instead, the combined action of compression, shear, and mechanical heterogeneity can promote extension in specific crustal volumes, particularly when stress perturbations are concentrated. In this context, unloading-induced reductions in σ_3 may act to further destabilize the local stress field, bringing portions of the crust closer to tensile failure even if the regional stress regime remains overall compressive. Accordingly, $\sigma_3 < 0$ conditions identified in our models should be interpreted as relative indicators of unloading-induced stress perturbations and mechanical favourability of tensile failure, rather than as universal or deterministic thresholds for magma ascent. While the present models do not explicitly resolve stress orientations or dyke trajectories under oblique loading, they capture the magnitude of unloading-related stress changes that may tip the balance between compression- and extension-dominated behaviour in mechanically heterogeneous volcanic systems.

The quadratic thinning function used in this study is useful to capture the general trend of increasing thinning. While real-world observations show greater variability and phase-specific accelerations (e.g., Zemp et al. 2022; Sommer et al. 2023), our simplified approach allows controlled comparisons between scenarios and isolates the mechanical effects of accelerated thinning-induced stress changes. To partially bridge this gap, we used observed elevation ranges and thinning constraints from Sollipulli volcano to motivate one end-member parameterized scenario. Nonetheless, future work could benefit from integrating glacier thinning curves derived from remote sensing or ice-flow models to further refine the temporal structure of surface unloading across a broader range of ice-capped and ice-filled volcanic systems.

Future work could explicitly incorporate realistic regional stress fields, high-resolution digital elevation models, detailed spatially resolved glacier thinning data, and laboratory-based measurements of the mechanical properties of crustal rocks in volcanic settings. Such efforts would help constrain the sensitivity of ice-capped volcanic systems, and particularly, glacier-filled calderas, to climate-driven changes in surface loading.

Conclusions

This study uses Finite Element Method models to investigate how progressive glacier unloading modifies the crustal stress field above pressurized magma bodies in ice-filled volcanic systems. Although the models are

Article in Press

idealized, assuming elastic rheology, axisymmetric geometry, prescribed pressure source depths, and simplified loading conditions, they capture first-order mechanical effects relevant to glacier-covered volcanoesThe depth of the magma body and the geometry of the overlying glacier exert a first-order control on the spatial distribution and sharpness of stress gradients. Shallow pressurized magma bodies experience stronger and more localized stress changes within a few hundred metres above the source roof, whereas deeper magma bodies show a more distributed tensile response over a thicker crustal column.

Our results show that cumulative ice mass loss systematically reduces the minimum principal stress (σ_3) in the upper crust above pressurized magma bodies and, in some configurations, drives a transition from compressive to tensile stress regimes. These stress transitions define domains where mode I fracturing is mechanically favoured, increasing the likelihood of vertical dyke propagation. Magma overpressure does not control the onset of tensile conditions by itself, particularly for deeper pressure sources, but it amplifies unloading-induced stress perturbations and increases the magnitude and vertical extent of tensile stresses once unloading progresses. Importantly, local inversions in σ_3 immediately above the source highlight that the region most favourable for tensile failure is not necessarily located at the pressure source margin, but within an overlying volume where stress gradients are maximized.

Within the linear elastic framework adopted here, the resulting stress state depends on the magnitude of glacier unloading, while the rate of ice thinning controls the timing at which a given stress condition is reached. Non-linear thinning histories, such as quadratic trajectories consistent with recent observations at Sollipulli in the Southern Volcanic Zone of the Andes, concentrate a large fraction of the total stress change into the later stages of , As a a pattern expected from the form of the prescribed thinning function itself. As a result, relatively small additional ice losses at advanced stages of deglaciation can produce disproportionately large stress perturbations, potentially advancing the onset of brittle failure and magma ascent. Consequently, glaciers that are already thin today could represent a disproportionately greater mechanical hazard than when they were intact.

Although motivated by the glacier-filled caldera of Sollipulli, the mechanical framework developed here is applicable to a wide range of volcanic systems hosting shallow or transient magma bodies, including those where long-term magma storage is deeper but short-lived intrusions develop in the upper crust. In such systems, climate-driven glacier retreat may progressively condition the stress state of the shallow crust, predisposing it to dyke propagation, fault reactivation, or eruptive activity once critical thresholds are approached. Future work

Article in Press

incorporating tectonic loads, viscoelastic rheologies, three-dimensional source geometries, realistic topography, evolving ice loads, and crustal heterogeneity will further refine these scenarios and improve assessments of how glacier retreat may interact with magmatic processes under ongoing and projected anthropogenic climate change.

Author contributions

MC: Conceptualization, Methodology, Software, Validation, Formal analysis, Investigation, Visualization, Writing-Original Draft, Writing-Review and Editing. HL: Conceptualization, Writing-Review and Editing. OK: Methodology, Data curation, Formal analysis, Writing-Review and Editing.

Acknowledgements

We thank Chiara Montagna for careful editorial guidance throughout the review process. We are also grateful to the two anonymous reviewers for their thoughtful and constructive comments, which helped clarify the scope of the study and strengthen the manuscript. We thank John Browning for providing access to COMSOL Multiphysics. This research did not receive any specific grant from funding agencies in the public, commercial, or not-for-profit sectors.

Data availability

The finite element model and elevation-change datasets supporting this study are openly available at Zenodo: 10.5281/zenodo.21393673 (Clunes et al., 2026). The repository includes the COMSOL Multiphysics finite element model (FEM folder) and elevation-change data derived from KH-9 Hexagon and Copernicus DEM imagery, together with the caldera boundary delineation used to constrain the study area (DEM folder). All other data supporting the findings of this study are available within the article and its supplementary material.

Article in Press

References

Albino, F., Pinel, V., and Sigmundsson, F. (2010). Influence of surface load variations on eruption likelihood: application to two Icelandic subglacial volcanoes, Grímsvötn and Katla. *Geophysical Journal International*, 181(3), 1510-1524. https://doi.org/10.1111/j.1365-246X.2010.04603.x

Ammirati, J. B., Azúa, K., Pastén-Araya, F., Richter, A., Wiens, D. A., Flores, M. C., Ruiz, S., Guzmán-Marín, P., Lanza, F., and Sielfeld, G. (2024). Fault reactivation linked to rapid ice-mass removal from the Southern Patagonian Icefield (48–52° S). *Tectonophysics*, 880, 230320. https://doi.org/10.1016/j.tecto.2024.230320

Arndt, J. E., Somos, M., Navas, S., Farías-Barahona, D., Rivera, A., Xie, H., & Fernández, A. (2026). The Decline of a caldera-filling glacier at Volcán Sollipulli, Chile. *Journal of Geophysical Research: Earth Surface*, 131, e2025JF008882. https://doi.org/10.1029/2025JF008882

Aubry, T. J., Farquharson, J. I., Rowell, C. R., Watt, S. F., Pinel, V., Beckett, F., Fasullo, J., Hopcroft, P., Pyle, D. M., Schmidt, A., and Sykes, J. S. (2022). Impact of climate change on volcanic processes: current understanding and future challenges. *Bulletin of Volcanology*, 84(6), 58. https://doi.org/10.1007/s00445-022-01562-8

Bahr, D. B., Pfeffer, W. T., and Kaser, G. (2015). A review of volume-area scaling of glaciers. *Reviews of Geophysics*, 53(1), 95-140. https://doi.org/10.1002/2014RG000470

Bonaccorso, A., Currenti, G., Del Negro, C., and Boschi, E. (2010). Dike deflection modelling for inferring magma pressure and withdrawal, with application to Etna 2001 case. *Earth and Planetary Science Letters*, 293(1-2), 121-129. https://doi.org/10.1016/j.epsl.2010.02.030

Brown, M. R., and Ge, S. (2018). Small earthquakes matter in injection-induced seismicity. *Geophysical Research Letters*, *45*(11), 5445-5453. https://doi.org/10.1029/2018GL077472

Carrivick, J. L., Davies, M., Wilson, R., Davies, B. J., Gribbin, T., King, O., Rabatel, A., García, J. K., and Ely, J. C. (2024). Accelerating glacier area loss across the Andes since the Little Ice Age. *Geophysical Research Letters*, 51(13). https://doi.org/10.1029/2024GL109154

Article in Press

Cashman, K. V., Sparks, R. S. J., and Blundy, J. D. (2017). Vertically extensive and unstable magmatic systems: a unified view of igneous processes. *Science*, *355*(6331), eaag3055. DOI: 10.1126/science.aag3055

Castro, J. M., Schipper, C. I., Mueller, S. P., Militzer, A. S., Amigo, A., Parejas, C. S., and Jacob, D. (2013). Storage and eruption of near-liquidus rhyolite magma at Cordón Caulle, Chile. *Bulletin of Volcanology*, *75*(4), 702. https://doi.org/10.1007/s00445-013-0702-9

Castro, J. M., Cordonnier, B., Schipper, C. I., Tuffen, H., Baumann, T. S., and Feisel, Y. (2016). Rapid laccolith intrusion driven by explosive volcanic eruption. *Nature Communications*, *7*(1), 13585. https://doi.org/10.1038/ncomms13585

Cembrano, J., and Lara, L. (2009). The link between volcanism and tectonics in the southern volcanic zone of the Chilean Andes: a review. *Tectonophysics*, *471*(1-2), 96-113. https://doi.org/10.1016/j.tecto.2009.02.038

Clunes, M., Browning, J., Cembrano, J., Marquardt, C., and Gudmundsson, A. (2021). Crustal folds alter local stress fields as demonstrated by magma sheet-fold interactions in the Central Andes. *Earth and Planetary Science Letters*, 570, 117080. https://doi.org/10.1016/j.epsl.2021.117080

Clunes, M., Browning, J., Marquardt, C., Cortez, J., Drymoni, K., and Kavanagh, J. (2023). Inclination and heterogeneity of layered geological sequences influence dike-induced ground deformation. *Geology*, 51(3), 278-283. https://doi.org/10.1130/G50464.1

Clunes, M., Browning, J., Cortez, J., Cembrano, J., Marquardt, C., Kavanagh, J. L., and Gudmundsson, A. (2024). Stresses induced by magma chamber pressurization altered by mechanical layering and layer dip. *Journal of Geophysical Research: Solid Earth*, 129(5), e2023JB027760. https://doi.org/10.1029/2023JB027760

Coonin, A. N., Huber, C., Troch, J., Townsend, M., Scholz, K., and Singer, B. S. (2024). Magma chamber response to ice unloading: Applications to volcanism in the West Antarctic rift system. *Geochemistry, Geophysics, Geosystems*, *25*(12), e2024GC011743. https://doi.org/10.1029/2024GC011743

Article in Press

Daros Idalino, F., Kellem da Rosa, K., Ferrando Acuña, F., Kozhikkodan Veettil, B., Cardia Simões, J., and Souza Jr, E. (2020). Recent glacier variations on Mount Melimoyu (44° 50'S-72° 51'W), Chilean Patagonia, using Sentinel-2 data. *Geocarto International*, 35(11), 1199-1213. https://doi.org/10.1080/10106049.2018.1557262

Davies, B. J., Darvill, C. M., Lovell, H., Bendle, J. M., Dowdeswell, J. A., Fabel, D., García, J. L., Geiger, A., Glasser, N. F., Gheorghiu, D. M., Harrison, S., Hein, A. S., Kaplan, M. R., Martin, J. R. V., Mendelova, M., Palmer, A., Pelto, M., Rodés, A., Sagredo, E. A., Smedley, R. K., and Thorndycraft, V. R. (2020). The evolution of the Patagonian Ice Sheet from 35 ka to the present day (PATICE). *Earth-Science Reviews*, 204, 103152. https://doi.org/10.1016/j.earscirev.2020.103152

Drymoni, K., Tibaldi, A., Bonali, F. L., and Mariotto, F. A. P. (2023). Dyke to sill deflection in the shallow heterogeneous crust during glacier retreat: part I. *Bulletin of Volcanology*, 85(12), 73. https://doi.org/10.1007/s00445-023-01684-7

Drymoni, K., Tibaldi, A., Bonali, F. L., and Mariotto, F. P. (2024). Dyke to sill deflection in the shallow heterogeneous crust during glacier retreat: part II. *Bulletin of Volcanology*, 86(5), 43. https://doi.org/10.1007/s00445-024-01732-w

Delgado, F., Pritchard, M. E., Basualto, D., Lazo, J., Córdova, L., and Lara, L. E. (2016). Rapid reinflation following the 2011–2012 rhyodacite eruption at Cordón Caulle volcano (Southern Andes) imaged by InSAR: Evidence for magma reservoir refill. *Geophysical Research Letters*, *43*(18), 9552-9562. https://doi.org/10.1002/2016GL070066

Delgado, F., Pritchard, M., Samsonov, S., and Córdova, L. (2018). Renewed posteruptive uplift following the 2011–2012 rhyolitic eruption of Cordón Caulle (Southern Andes, Chile): Evidence for transient episodes of magma reservoir recharge during 2012–2018. *Journal of Geophysical Research: Solid Earth*, 123(11), 9407-9429. https://doi.org/10.1029/2018JB016240

Dussaillant, I., Berthier, E., Brun, F., Masiokas, M., Hugonnet, R., Favier, V., Rabatel, A., Pitte, P., and Ruiz, L. (2019). Two decades of glacier mass loss along the Andes, *Nature Geosciences*, 12, 802–808. https://doi.org/10.1038/s41561-019-0432-5

Article in Press

Ferrante, G., Rivalta, E., and Maccaferri, F. (2024). Spatio-temporal evolution of rift volcanism controlled top-down by a deepening graben. *Earth and Planetary Science Letters*, *629*, 118593. https://doi.org/10.1016/j.epsl.2024.118593

Freundt, A., Strehlow, K., Kutterolf, S., and Schindlbeck-Belo, J. C. (2025). Magmatic evolution and magma chamber conditions of the Alpehué tephra from Sollipulli Volcano, Andean Southern Volcanic Zone, Chile/Argentina. *Contributions to Mineralogy and Petrology*, *180*(1), 3. https://doi.org/10.1007/s00410-024-02195-0

Galland, O., Burchardt, S., Hallot, E., Mourgues, R., and Bulois, C. (2014). Dynamics of dikes versus cone sheets in volcanic systems. *Journal of Geophysical Research: Solid Earth*, 119(8), 6178-6192. https://doi.org/10.1002/2014JB011059

Gardner, J. V., Dartnell, P., Hellequin, L., Bacon, C. R., Mayer, L. A., Buktenica, M. W., and Stone, J. C. (2001). Bathymetry and selected perspective views of Crater Lake, Oregon. *Water-Resources Investigations Report*, *1*, 4046.

Gilbert, J. S., Stasiuk, M. V., Lane, S. J., Adam, C. R., Murphy, M. D., Sparks, R. S. J., and Naranjo, J. A. (1996). Non-explosive, constructional evolution of the ice-filled caldera at Volcán Sollipulli, Chile. *Bulletin of Volcanology*, 58, 67-83. https://doi.org/10.1007/s004450050127

Glazner, A.F., Manley, C.R., Marron, J.S., and Rojstaczer, S. (1999). Fire or ice: anticorrelation of volcanism and glaciation in California over the past 800,000 years. *Geophysical Research Letters*, 26, 1759–1762. https://doi.org/10.1029/1999GL900333

Gudmundsson, A. (2002). Emplacement and arrest of sheets and dykes in central volcanoes. *Journal of Volcanology and Geothermal Research*, 116(3-4), 279-298. https://doi.org/10.1016/S0377-0273(02)00226-3

Gudmundsson, A., and Brenner, S. L. (2004). How mechanical layering affects local stresses, unrests, and eruptions of volcanoes. *Geophysical Research Letters*, 31(16). https://doi.org/10.1029/2004GL020083

Article in Press

Gudmundsson, A. (2006). How local stresses control magma-chamber ruptures, dyke injections, and eruptions in composite volcanoes. *Earth-Science Reviews*, 79(1-2), 1-31. https://doi.org/10.1016/j.earscirev.2006.06.006

Gudmundsson, A. (2011). Rock fractures in geological processes. Cambridge University Press.

Heap, M. J., and Violay, M. E. (2021). The mechanical behaviour and failure modes of volcanic rocks: a review. *Bulletin of Volcanology*, 83(5), 33. https://doi.org/10.1007/s00445-021-01447-2

Hickey, J., and Gottsmann, J. (2014). Benchmarking and developing numerical Finite Element models of volcanic deformation. *Journal of Volcanology and Geothermal Research*, 280, 126-130. https://doi.org/10.1016/j.jvolgeores.2014.05.011

Hill, D. P., Pollitz, F., and Newhall, C. (2002). Earthquake–volcano interactions. *Physics Today*, 55(11), 41-47. https://doi.org/10.1063/1.1535006

Hooper, A., Ófeigsson, B., Sigmundsson, F., Lund, B., Einarsson, P., Geirsson, H., and Sturkell, E. (2011). Increased capture of magma in the crust promoted by ice-cap retreat in Iceland. *Nature Geoscience*, 4(11), 783-786. https://doi.org/10.1038/ngeo1269

Hugonnet, R., McNabb, R., Berthier, E., Menounos, B., Nuth, C., Girod, L., Farinotti, D., Huss, M., Dussaillant, I., Brun, F., and Kääb, A. (2021). Accelerated global glacier mass loss in the early twenty-first century. *Nature*, 592(7856), 726-731. https://doi.org/10.1038/s41586-021-03436-z

Hugonnet, R., Brun, F., Berthier, E., Dehecq, A., Mannerfelt, E. S., Eckert, N., and Farinotti, D. (2022). Uncertainty analysis of digital elevation models by spatial inference from stable terrain. *IEEE Journal of Selected Topics in Applied Earth Observations and Remote Sensing*, 15, 6456-6472. 10.1109/JSTARS.2022.3188922

Huybers, P., and Langmuir, C. (2009). Feedback between deglaciation, volcanism, and atmospheric CO_2. Earth and Planetary Science Letters, 286(3-4), 479-491. https://doi.org/10.1016/j.epsl.2009.07.014

Article in Press

Jellinek, A. M., Manga, M., and Saar, M. O. (2004). Did melting glaciers cause volcanic eruptions in eastern California? Probing the mechanics of dike formation. *Journal of Geophysical Research: Solid Earth*, 109(B9). https://doi.org/10.1029/2004JB002978

Jó, V., de Vries, M. V. W., Ignéczi, Á., Mari, L., and Nagy, B. (2023). Glacier slowdown and rapid ice loss in the Tinguiririca and Cachapoal Basin, Central Andes of Chile. *Global and Planetary Change*, 231, 104287. https://doi.org/10.1016/j.gloplacha.2023.104287

King, G. C. P., Stein, R. S., and Lin, J. (1994). Static stress changes and the triggering of earthquakes. Bulletin of the Seismological Society of America, 84(3), 935–953. https://doi.org/10.1785/BSSA0840030935

Kratzmann, D. J., Carey, S., Scasso, R., and Naranjo, J. A. (2009). Compositional variations and magma mixing in the 1991 eruptions of Hudson volcano, Chile. *Bulletin of Volcanology*, 71(4), 419-439. https://doi.org/10.1007/s00445-008-0234-x

Maccaferri, F., Rivalta, E., Keir, D., and Acocella, V. (2014). Off-rift volcanism in rift zones determined by crustal unloading. *Nature Geoscience*, *7*(4), 297-300. https://doi.org/10.1038/ngeo2110

Martínez, P., Singer, B. S., Roa, H. M., and Jicha, B. R. (2018). Volcanologic and petrologic evolution of Antuco-Sierra Velluda, southern Andes, Chile. *Journal of Volcanology and Geothermal Research*, 349, 392-408. https://doi.org/10.1016/j.jvolgeores.2017.11.026

Masiokas, M. H., Rabatel, A., Rivera, A., Ruiz, L., Pitte, P., Ceballos, J. L., Barcaza, G., Soruco, A., Bown, F., Berthier, E., Dussaillant, I., and MacDonell, S. (2020). A review of the current state and recent changes of the Andean cryosphere. *Frontiers in Earth Science*, 8, 99. https://doi.org/10.3389/feart.2020.00099

Mendelova, M., Hein, A. S., McCulloch, R., and Davies, B. (2017). The last glacial maximum and deglaciation in central Patagonia, 44° S–49° S. *Cuadernos de Investigación Geográfica*, 43(2), 719-750. https://doi.org/10.18172/cig.3263

Article in Press

Mogi, K. (1958). Relations between the eruptions of various volcanoes and the deformations of the ground surfaces around them. *Bulletin of the Earthquake Research Institute*, 36(99), pp. 99-134.

Mouginot, J., and Rignot, E. (2015). Ice motion of the Patagonian icefields of South America: 1984–2014. *Geophysical Research Letters*, 42(5), 1441-1449. https://doi.org/10.1002/2014GL062661

Mora, D., and Tassara, A. (2019). Upper crustal decompression due to deglaciation-induced flexural unbending and its role on post-glacial volcanism at the Southern Andes. *Geophysical Journal International*, *216*(3), 1549-1559. https://doi.org/10.1093/gji/ggy473

Moreno-Yaeger, P., Singer, B. S., Edwards, B. R., Jicha, B. R., Nachlas, W. O., Kurz, M. D., Breunig, R. E., Fustos-Toribio, I., Vásquez Antipán, D., and Piergrossi, E. (2024). Pleistocene to recent evolution of Mocho-Choshuenco volcano during growth and retreat of the Patagonian Ice Sheet. *Geological Society of America Bulletin*, 136(11-12), 5262-5282. https://doi.org/10.1130/B37514.1

Moreno-Yaeger, P., Singer, B. S., Alloway, B. V., Townsend, M., Cuzzone, J., Nachlas, W. O., Edwards, B. R., Jicha, B., Marcott, S. A., and Boschetty, F. O. (2025). Expansion and contraction of the Patagonian ice sheet and its influence on magma storage beneath Mocho-Choshuenco volcano, Chile. *Journal of Geophysical Research: Solid Earth*, 130(10), e2025JB031528. https://doi.org/10.1029/2025JB031528

Naranjo, J. A., Moreno, H., Emparan, C., and Murphy, M. (1993). Volcanismo explosivo reciente en la caldera del volcán Sollipulli, Andes del Sur (39 S). *Andean Geology*, 20(2), 167-191.

Lachowycz, S. M., Pyle, D. M., Gilbert, J. S., Mather, T. A., Mee, K., Naranjo, J. A., and Hobbs, L. K. (2015). Glaciovolcanism at Volcán Sollipulli, southern Chile: Lithofacies analysis and interpretation. *Journal of Volcanology and Geothermal Research*, *303*, 59-78. https://doi.org/10.1016/j.jvolgeores.2015.06.021

Long, S. M., and Grosfils, E. B. (2009). Modeling the effect of layered volcanic material on magma reservoir failure and associated deformation, with application to Long Valley caldera, California. Journal of Volcanology and Geothermal Research, 186(3-4), 349-360. https://doi.org/10.1016/j.jvolgeores.2009.05.021

Article in Press

Pagli, C., and Sigmundsson, F. (2008). Will present day glacier retreat increase volcanic activity? Stress induced by recent glacier retreat and its effect on magmatism at the Vatnajökull ice cap, Iceland. *Geophysical Research Letters*, 35(9). https://doi.org/10.1029/2008GL033510

Pelto, M. S. (2010). Forecasting temperate alpine glacier survival from accumulation zone observations. *The Cryosphere*, 4(1), 67-75. https://doi.org/10.5194/tc-4-67-2010

Pinel, V., and Jaupart, C. (2005). Some consequences of volcanic edifice destruction for eruption conditions. *Journal of Volcanology and Geothermal Research*, 145(1-2), 68-80. https://doi.org/10.1016/j.jvolgeores.2005.01.012

Pinel, V., Sigmundsson, F., Sturkell, E., Geirsson, H., Einarsson, P., Gudmundsson, M. T., and Högnadóttir, T. (2007). Discriminating volcano deformation due to magma movements and variable surface loads: application to Katla subglacial volcano, Iceland. *Geophysical Journal International*, 169(1), 325-338. https://doi.org/10.1111/j.1365-246X.2006.03267.x

Praetorius, S., Mix, A., Jensen, B., Froese, D., Milne, G., Wolhowe, M., Addison, J., and Prahl, F. (2016). Interaction between climate, volcanism, and isostatic rebound in Southeast Alaska during the last deglaciation. *Earth and Planetary Science Letters*, 452, 79-89. https://doi.org/10.1016/j.epsl.2016.07.033

Rabatel, A., Francou, B., Soruco, A., Gomez, J., Cáceres, B., Ceballos, Basantes, R., Vuille, M., Sicart, J. E., Huggel, C., Scheel, M., Lejeune, Y., Arnaud, Y., Collet, M., Condom, T., Consoli, G., Favier, V., Jomelli, V., Galarraga, R., Ginot, P., Maisincho, L., Mendoza, J., Ménégoz, M., Ramirez, E., Ribstein, P., Suarez, W., Villacis, M., and Wagnon, P. (2013). Current state of glaciers in the tropical Andes: a multi-century perspective on glacier evolution and climate change. *The Cryosphere*, 7(1), 81-102. https://doi.org/10.5194/tc-7-81-2013

Rawson, H., Naranjo, J. A., Smith, V. C., Fontijn, K., Pyle, D. M., Mather, T. A., and Moreno, H. (2015). The frequency and magnitude of post-glacial explosive eruptions at Volcán Mocho-Choshuenco, southern Chile. *Journal of Volcanology and Geothermal Research*, *299*, 103-129. https://doi.org/10.1016/j.jvolgeores.2015.04.003

Article in Press

Rawson, H., Pyle, D. M., Mather, T. A., Smith, V. C., Fontijn, K., Lachowycz, S. M., and Naranjo, J. A. (2016). The magmatic and eruptive response of arc volcanoes to deglaciation: Insights from southern Chile. *Geology*, *44*(4), 251-254. https://doi.org/10.1130/G37504.1

Reinthaler, J., Paul, F., Granados, H. D., Rivera, A., and Huggel, C. (2019). Area changes of glaciers on active volcanoes in Latin America between 1986 and 2015 observed from multi-temporal satellite imagery. *Journal of Glaciology*, 65(252), 542-556. https://doi.org/10.1017/jog.2019.30

RGI 7.0 Consortium. (2023). Randolph Glacier Inventory - A Dataset of Global Glacier Outlines, Version 7.0. Boulder, Colorado USA. NSIDC: *National Snow and Ice Data Center*. https://doi.org/10.5067/f6jmovy5navz

Richter, A., Ivins, E., Lange, H., Mendoza, L., Schröder, L., Hormaechea, J. L., Casassa, G., Marderwald, E., Fritsche, M., Perdomo, R., Horwarth, M., Dietrich, R., and Dietrich, R. (2016). Crustal deformation across the Southern Patagonian Icefield observed by GNSS. *Earth and Planetary Science Letters*, 452, 206-215. https://doi.org/10.1016/j.epsl.2016.07.042

Rivalta, E., and Chamberlain, K. (2025). The influence of crustal stress on the pathways and evolution of magmas ascending by dyking. *Authorea Preprints*. 10.22541/essoar.175241977.71415284/v1

Rivera, A., Bown, F., Mella, R., Wendt, J., Casassa, G., Acuña, C., Rignot, E., Clavero, J., and Brock, B. (2006). Ice volumetric changes on active volcanoes in southern Chile. Annals of Glaciology, 43, 111-122. https://doi:10.3189/172756406781811970

Rivera, A., and Bown, F. (2013). Recent glacier variations on active ice capped volcanoes in the Southern Volcanic Zone (37–46 S), Chilean Andes. *Journal of South American Earth Sciences*, 45, 345-356. https://doi.org/10.1016/j.jsames.2013.02.004

Roman, D. C., and Cashman, K. V. (2018). Top–down precursory volcanic seismicity: implications for 'Stealth' magma ascent and long-term eruption forecasting. *Frontiers in Earth Science*, 6, 124. https://doi.org/10.3389/feart.2018.00124

Article in Press

Romero, J. E., Polacci, M., Arzilli, F., Schipper, C. I., La Spina, G., Burton, M., Parada, M. A., Norambuena, J., Guevara, A., Watt, S., Moreno, H., Framco, L., and Fellowes, J. (2023). Long-term volcano evolution controlled by lateral collapse at Antuco volcano, southern Andes, Chile. *Communications Earth and Environment*, 4(1), 292. https://doi.org/10.1038/s43247-023-00931-1

Rubin, A. M. (1995). Propagation of magma-filled cracks. *Annual Review Of Earth And Planetary Sciences*, Volume 23, pp. 287-336., 23, 287-336.

Rupnik, E., Daakir, M., and Pierrot Deseilligny, M. (2017). MicMac–a free, open-source solution for photogrammetry. *Open geospatial data, software and standards*, 2(1), 14. https://doi.org/10.1186/s40965-017-0027-2

Ruz, J., Browning, J., Cembrano, J., Iturrieta, P., Gerbault, M., and Sielfeld, G. (2020). Field observations and numerical models of a Pleistocene-Holocene feeder dyke swarm associated with a fissure complex to the east of the Tatara-San Pedro-Pellado complex, Southern Volcanic Zone, Chile. *Journal of Volcanology and Geothermal Research*, 404, 107033. https://doi.org/10.1016/j.jvolgeores.2020.107033

Satow, C., Gudmundsson, A., Gertisser, R., Ramsey, C. B., Bazargan, M., Pyle, D. M., Wulf, S., Miles, A. J., and Hardiman, M. (2021). Eruptive activity of the Santorini Volcano controlled by sea-level rise and fall. *Nature Geoscience*, *14*(8), 586-592. https://doi.org/10.1038/s41561-021-00783-4

Seropian, G., Schipper, C. I., Harmon, L. J., Smithies, S. L., Kennedy, B. M., Castro, J. M., Alloway, B. V., and Forte, P. (2021). A century of ongoing silicic volcanism at Cordón Caulle, Chile: New constraints on the magmatic system involved in the 1921–1922, 1960 and 2011–2012 eruptions. *Journal of Volcanology and Geothermal Research*, *420*, 107406. https://doi.org/10.1016/j.jvolgeores.2021.107406

Sigmundsson, F., Pinel, V., Lund, B., Albino, F., Pagli, C., Geirsson, H., and Sturkell, E. (2010). Climate effects on volcanism: influence on magmatic systems of loading and unloading from ice mass variations, with examples from Iceland. *Philosophical Transactions of the Royal Society A: Mathematical, Physical and Engineering Sciences*, 368(1919), 2519-2534. https://doi.org/10.1098/rsta.2010.0042

Article in Press

Sigmundsson, F., Albino, F., Schmidt, P., Lund, B., Pinel, V., Hooper, A., and Pagli, C. (2013). Multiple effects of ice load changes and associated stress change on magmatic systems. *Climate Forcing of Geological and Geomorphological Hazards*, 108-123.

Sigvaldason, G. E., Annertz, K., and Nilsson, M. (1992). Effect of glacier loading/deloading on volcanism: postglacial volcanic production rate of the Dyngjufjöll area, central Iceland. *Bulletin of Volcanology*, 54, 385-392. https://doi.org/10.1007/BF00312320

Singer, B., Hildreth, W., and Vincze, Y. (2000). $^{40}Ar/^{39}Ar$ evidence for early deglaciation of the central Chilean Andes. *Geophysical Research Letters*, 27(11), 1663-1666. https://doi.org/10.1029/1999GL011065

Singer, B. S., Moreno-Yaeger, P., Townsend, M., Huber, C., Cuzzone, J., Edwards, B. R., Romero, M., Orellana-Salazar, Y., Marcott, S. A., Breunig, R. E., Ferrier, K. L., Scholz, K., Coonin, A. N., Alloway, B. V., Tremblay, M. M., Stevens, S., Fustos-Toribio, I., Moreno, P., Vera, F., and Amigo, Á. (2024). New perspectives on ice forcing in continental arc magma plumbing systems. *Journal of Volcanology and Geothermal Research*, *455*, 108187. https://doi.org/10.1016/j.jvolgeores.2024.108187

Sommer, C., Fürst, J. J., Huss, M., and Braun, M. H. (2023). Constraining regional glacier reconstructions using past ice thickness of deglaciating areas–a case study in the European Alps. *The Cryosphere Discussions*, 2022, 1-30. https://doi.org/10.5194/tc-17-2285-2023

Sottili, G., and Palladino, D. M. (2025). When volcanoes record Milankovitch cycles. *Frontiers in Earth Science*, *13*, 1569128. https://doi.org/10.3389/feart.2025.1569128

Swain, B., Vountas, M., Singh, A., and Gunthe, S. S. (2024). Tracing human influence on rising surface air temperature in Venezuela. *Scientific Reports*, 14(1), 28005. https://doi.org/10.1038/s41598-024-79671-x

The GlaMBIE Team. Community estimate of global glacier mass changes from 2000 to 2023. *Nature* 639, 382–388 (2025). https://doi.org/10.1038/s41586-024-08545-z

Article in Press

Toda, S., Stein, R. S., Richards-Dinger, K., and Bozkurt, S. B. (2005). Forecasting the evolution of seismicity in southern California: Animations built on earthquake stress transfer. *Journal of Geophysical Research: Solid Earth*, 110(B5). https://doi.org/10.1029/2004JB003415

Trasatti, E., Giunchi, C., and Bonafede, M. (2003). Effects of topography and rheological layering on ground deformation in volcanic regions. *Journal of Volcanology and Geothermal Research*, 122(1-2), 89-110. https://doi.org/10.1016/S0377-0273(02)00473-0

Tuffen, H. (2010). How will melting of ice affect volcanic hazards in the twenty-first century?. *Philosophical Transactions of the Royal Society A: Mathematical, Physical and Engineering Sciences*, 368(1919), 2535-2558. https://doi.org/10.1098/rsta.2010.0063

Van Wyk de Vries, M., Bingham, R. G. and Hein, A. S. (2018). A new volcanic province: an inventory of subglacial volcanoes in West Antarctica. *Geol. Soc. London Spl. Publ.* 461, (231–248). https://doi.org/10.1144/SP461.7

Van Wyk de Vries, M., Carchipulla-Morales, D., Wickert, A. D., and Minaya, V. G. (2022). Glacier thickness and ice volume of the Northern Andes. *Scientific Data*, 9(1), 342. https://doi.org/10.1038/s41597-022-01446-8

Villarroel, M., Browning, J., Marquardt, C., Clunes, M., Zañartu, G., and Giordano, G. (2024). Reconciling mechanical models of caldera ring-fault nucleation within the transcrustal magmatic system paradigm. *Journal of Volcanology and Geothermal Research*, 449, 108073. https://doi.org/10.1016/j.jvolgeores.2024.108073

Wang, W., Li, S., Wei, H., Zhao, Z., Wang, H., and He, X. (2025). Glacial melting accelerates andean uplift: Insights from 2D viscoelastic-plastic subduction models. *Earth and Planetary Science Letters*, 662, 119386. https://doi.org/10.1016/j.epsl.2025.119386

Wanket, S., Jellinek, A. M., and Johnson, C. L. (2025). Potential ice sheet modulation of volcanism in West Antarctica: Constraints on the cadence and magnitude of melt delivery into the crust. *Journal of Geophysical Research: Solid Earth*, *130*(6), e2024JB029730. https://doi.org/10.1029/2024JB029730

Article in Press

Watt, S. F., Pyle, D. M., and Mather, T. A. (2013). The volcanic response to deglaciation: Evidence from glaciated arcs and a reassessment of global eruption records. *Earth-Science Reviews*, 122, 77-102. https://doi.org/10.1016/j.earscirev.2013.03.007

Wilson, A. M., and Russell, J. K. (2020). Glacial pumping of a magma-charged lithosphere: a model for glaciovolcanic causality in magmatic arcs. *Earth and Planetary Science Letters*, *548*, 116500. https://doi.org/10.1016/j.epsl.2020.116500

xDEM contributors. (2023). xDEM (v0.0.18). Zenodo. https://doi.org/10.5281/zenodo.11204531

Zekollari, H., Schuster, L., Maussion, F., Hock, R., Marzeion, B., Rounce, D. R., Compagno, L., Fujita, K., Huss, M., James, M., Kraaijenbrink, P. D. A., Lipscomb, W. H., Minallah, S., Oberrauch, M., Van Tricht, L., Champollion, N., Edwards, T., Farinotti, D., Immerzeel, W., Leguy, G., and Sakai, A. (2025). Glacier preservation doubled by limiting warming to 1.5° C versus 2.7° C. *Science*, 388(6750), 979-983. https://www.science.org/doi/abs/10.1126/science.adu4675

Zemp, M., Huss, M., Thibert, E., Eckert, N., McNabb, R., Huber, J., Barandun, M., Machguth, H., Nussbaumer, S. U., Gärtner-Roer, I., Thomson, L., Paul, F., Maussion, F., Kutuzov, S., and Cogley, J. G. (2019). Global glacier mass changes and their contributions to sea-level rise from 1961 to 2016. *Nature*, 568(7752), 382-386. https://doi.org/10.1038/s41586-019-1071-0

Ziv, A., and Rubin, A. M. (2000). Static stress transfer and earthquake triggering: No lower threshold in sight? Journal of Geophysical Research:Solid Earth, 105, 13,631–13,642. https://doi.org/10.1029/2000JB900081

Article in Press